
**Experimental determination of the extent of Fe(III)
reduction and Fe isotope fractionation during
microbial reduction of ferrihydrite in freshwater
systems by sulfate-reducing bacteria**

by

Yan Zhang

A thesis

presented to the University of Waterloo

in fulfillment of the

thesis requirement for the degree of

Master of Science

in

Earth Sciences

Waterloo, Ontario, Canada, 2017

© Yan Zhang 2017

Author's Declaration

I hereby declare that I am the sole author of this thesis. This is a true copy of the thesis, including any required final revisions, as accepted by my examiners.

I understand that my thesis may be made electronically available to the public.

Abstract

Traditionally, sulfur was thought to have little influence on Fe cycling in freshwater systems because of the low sulfate concentrations (average ~ 0.2 mM) in such waters. However, a recent study suggested that a cryptic sulfur cycle exists for freshwater systems, as it does in more sulfate-rich marine environments. Therefore, sulfur cycling could be a driving factor of Fe redox cycling even in low-sulfate conditions. To test the hypothesis that cryptic sulfur cycling significantly influences Fe cycling in sulfate-poor freshwater environments, this study reports Fe concentration and isotope data during sulfide-induced Fe reduction and direct enzymatic Fe reduction by two sulfate-reducing bacteria (SRB): *Desulfovibrio vulgaris* (*D. vulgaris*), which is capable of reducing chelated Fe(III) as well as insoluble Fe(III) oxides enzymatically, and *Desulfohalobium curvatum* (*D. curvatum*), which cannot enzymatically reduce Fe(III).

Four experimental sets were performed to infer the main controls on the extent of Fe(III) reduction: (i) 0.2 mM abiotic sulfide and Si and ferrihydrite co-precipitates (Si-HFO) (ii) SRB (*D. vulgaris*) and Si-HFO, (iii) 0.2 mM enzymatically produced sulfide (from *D. vulgaris* or *D. curvatum*) and Si-HFO with the absence of *D. vulgaris*, and (iv) 0.2 mM sulfate, SRB (*D. vulgaris* or *D. curvatum*), and Si-HFO. The abiotic and enzymatically produced sulfide experiments yielded similar extents of Fe(III) reduction. By contrast, direct enzymatic Fe(III) reduction by SRB (*D. vulgaris*) was less efficient. The experiment with SRB and Si-HFO in the presence of sulfate had the highest extent of Fe(III) reduction. This extent is higher than the total of simply (ii) plus (iii), thus confirming the presence of a cryptic S cycle at low-sulfate conditions.

To investigate how SRB influences Fe isotope fractionation during Fe(III) reduction, two experiment sets were performed: (i) SRB (*D. vulgaris*) and 0.7 mM Si-HFO, and (ii) 0.2 mM enzymatically produced sulfide (from *D. vulgaris*) and 0.7 mM Si-HFO. With increased extent of Fe(III) reduction, $\delta^{56}\text{Fe}_{\text{aq}}$ significantly increased, $\delta^{56}\text{Fe}_{\text{solid}}$ slightly increased, and $\delta^{56}\text{Fe}_{\text{sorb}}$ slightly decreased. The most positive and negative $\delta^{56}\text{Fe}$ values were $0.48 \pm 0.48\text{‰}$ (2σ ; $n = 6$) and $-1.39 \pm 1.30\text{‰}$ (2σ ; $n = 6$) in the solid phase and aqueous phase, respectively, from the experiment with enzymatically produced sulfide. The Fe isotope fractionation between $\text{Fe(II)}_{\text{aq}}$ and $\text{Fe(III)}_{\text{solid}}$ ($\Delta^{56}\text{Fe}_{\text{Fe(II)}_{\text{aq}}-\text{Fe(III)}_{\text{solid}}}$) in both experiments was inversely correlated with the extent of Fe(III) reduction during the duration of the experiments (20 days). However, based on previous studies,

equilibrium Fe isotope fractionation was expected for redox changes. Thus, if a longer experiment had been performed, the Fe isotopes may have continued to exchange until the system reached equilibrium. The $\Delta^{56}\text{Fe}_{\text{Fe(II)aq}-\text{Fe(III)solid}}$ in the experiments with enzymatically produced sulfide and with SRB (*D. vulgaris*) ranged from -1.22‰ to -4.14‰ with an average of $-2.92 \pm 2.60\text{‰}$ (2σ ; $n = 4$), and from -0.04 to -0.86‰ with an average of $-0.39 \pm 0.68\text{‰}$ (2σ ; $n = 4$), respectively. From previous studies, $\Delta^{56}\text{Fe}_{\text{Fe(II)aq}-\text{Fe(III)solid}}$ was $\sim -3\text{‰}$ with the presence of dissimilatory Fe reducing bacteria (DIRB) (such as *Shewanella oneidensis* and *Geobacter sulfurreducens*). Hence, Fe isotope fractionation by enzymatically produced sulfide is similar to that observed for DIRB or abiotic systems whereas Fe isotope fractionation by SRB is significantly smaller. This study confirms that the same mechanism of Fe isotope fractionation occurs during dissimilatory Fe reduction (DIR) regardless of Fe substrate, but a different mechanism of Fe isotope fractionation occurs during DIR caused by SRB compared to DIRB. This result further suggests that Fe isotopes have the potential to be applied as a tracer to evaluate different microbial pathways for Fe(III) reduction, specifically: 1) enzymatically by SRB versus enzymatically by DIRB; and 2) enzymatically by SRB versus non-enzymatically by sulfide.

Acknowledgements

I would like to express my sincere gratitude and respect to my committee member and former supervisor, Dr. Lingling Wu for her expertise, guidance, and patience. The knowledge and research methods she taught will benefit me in further research on biogeochemistry. The successful and final outcome of this thesis could not have been achieved without her insightful knowledge, precious guidance, and assistance on both writing and lab work.

I also owe a deep sense of thanks to my formal supervisor and former committee member Dr. Brian Kendall for his understanding and encouragement. I have always been touched by his kindness and dedication to help students. He helped me greatly with writing the thesis and preparing for the thesis defense.

I also would like to express my sense of gratitude and indebtedness to my committee member Dr. Shaun Frape for providing me valuable feedback that greatly improved my thesis.

I would like to thank Dr. Deng Liu from China University of Geosciences, Wuhan, China for providing the culture of *Desulfovibrio vulgaris* ATCC29579.

I am grateful to my lab manager, Dr. Liyan Xing, for her kind help that ensured the smooth running of my laboratory work.

Kai Liu is thanked for assistance with Fe isotope measurements. I benefited a lot from his guidance, especially when doing the Fe column chemistry.

Dr. Clark Johnson and Dr. Brian Beard are thanked for generous access to their mass spectrometer at the University of Wisconsin-Madison.

I really appreciate Dr. Christina M. Smeaton and Bingjie Shi for their timely advice and insightful ideas throughout every stage of my research.

Finally, I would also like to thank the following colleagues and school mates for their love and support (including but not limited to): Jackson Makoto Tsuji, Jieying Wang, Ryan Truong,

Shuai Yang, Su Wang, and Xinze Lu.

This research was supported by NSERC Discovery Grants to Dr. Lingling Wu and Dr. Brian Kendall, and an Ontario Early Researcher Award to Dr. Lingling Wu.

Table of Content

Author's Declaration	ii
Abstract.....	iii
Acknowledgements	v
Table of Content.....	vii
List of Figures.....	ix
List of Tables	xi
1.0 Introduction.....	1
2.0 Background	8
2.1 Fe isotopes.....	8
2.2 <i>Desulfovibrio vulgaris</i> & <i>Desulfobacter curvatus</i>	10
3.0 Methodology	11
3.1 Experimental designs.....	11
3.2 Source of organisms and culturing techniques	13
3.2.1 Growth media.....	13
3.2.2 Cultivation techniques	15
3.2.3 Cell counting.....	16
3.3 Standard curve preparation & elemental concentration measurement	17
3.3.1 Fe standard curve and measurement.....	17
3.3.2 S Standard curve and measurement	20
3.3.3 Si standard curve and measurement.....	25
3.4 Sequential Fe extraction	26
3.5 Fe isotope measurement	27
4.0 Results & Discussion.....	30
4.1 Growth curves for <i>Desulfobacter curvatus</i> & <i>Desulfovibrio vulgaris</i>	30
4.2 Elemental concentrations	31

4.3 Fe isotope compositions 39

5.0 Conclusions 47

6.0 References 49

Appendix A - Supplementary Information..... 63

List of Figures

Figure 1. Microbial respiratory sequences with the sediments collected from Ashumet Pond, Falmouth, MA, USA.....	4
Figure 2. Cryptic S cycle during Fe(III) reduction.....	5
Figure 3. Color indicator for O ₂ concentrations in growth mediums with resazurin. ..	15
Figure 4. Growth cultures of <i>D. curvatus</i> with different optical density.	16
Figure 5. The effect of pH on the formation of the ferrous complex of ferrozine.....	18
Figure 6. The visible absorption spectrum of the ferrous complex of ferrozine.....	19
Figure 7. Fe(II) / Fe(tot) standard curves (at 562 nm).....	20
Figure 8. S calibration curves with different ranges of S concentration.	21
Figure 9. The effect of temperature on the colorimetric reagents.....	23
Figure 10. S standard curves for different S concentration ranges.	24
Figure 11. Si calibration standard curve (at 670 nm).....	26
Figure 12. Three step sequential extraction of aqueous, sorbed, and solid Fe fractions.	27
Figure 13. Sample picture of fluorescing <i>D. curvatus</i>	30
Figure 14. Sample picture of fluorescing <i>D. vulgaris</i>	30
Figure 15. Growth curve for <i>D. curvatus</i>	31
Figure 16. Growth curve for <i>D. vulgaris</i>	31
Figure 17. Changes in sulfide concentrations for different experimental sets.	33

Figure 18. Fe(II) concentration over time in different experimental sets..... 33

Figure 19. Extent of Fe(III) reduction by either *D. vulgaris* or the equivalent amount of sulfide produced by *D. vulgaris*, for different concentrations of Si-HFO..... 34

Figure 20. Fe(II) concentrations in all phases over time in different experimental sets. 35

Figure 21. Fe(tot) concentrations in all phases over time in different experimental sets. 36

Figure 22. Changes in the extent of Fe(III) reduction over time in different experimental sets. 36

Figure 23. Sample pictures of different experimental sets over time..... 37

Figure 24. Changes in Fe speciation in aqueous, sorbed, and solid phases over time... 38

Figure 25. Fe isotope fractionation among different Fe pools. 40

Figure 26. $\delta^{56}\text{Fe}$ among different Fe phases versus the extent of Fe reduction in a) set 7 and b) set 4. 41

Figure 27. Fe isotopic fractionation between $\text{Fe(II)}_{\text{aq}}$ and $\text{Fe(III)}_{\text{solid}}$ 44

List of Tables

Table 1. Geochemical analyses of flow-through experiments.....	2
Table 2. Gibbs free energy for reduction of Fe(III) and sulfate.	3
Table 3. Fe isotope compositions in natural environments.	9
Table 4. Experimental Designs.	13
Table 5. Suggested Fe concentration for Fe standard curve.....	18
Table 6. Suggested S concentration intervals for sulfur standards with different S concentration ranges.	21
Table 7. Suggested reagent concentrations for sulfide-sulfur analysis for different sulfide concentrations.	22
Table 8. Suggested Si concentrations for Si calibration standards.	25
Table 9. Fe isotope compositions of different Fe pools.	40

1.0 Introduction

It is not surprising that iron (Fe), the fourth most abundant element in the Earth's crust, has been extensively studied by many scientists (Beard & Johnson, 2004; Dauphas et al., 2017; Johnson et al., 2004; Kendall et al., 2012; Taylor & McLennan, 1985). The biogeochemical cycle of Fe is essential in studies of near-surface environments because many redox-sensitive and bioessential elements, including carbon, oxygen, nitrogen, and sulfur, are closely affected by the electron transfer processes during Fe redox transformations (Lalonde et al., 2012; Yao & Millero, 1996; Thamdrup et al., 1994).


Generally, the concentration of sulfate in today's ocean is approximately 28 mM (Canfield, 2004) whereas, according to a global network of water monitoring stations, freshwater contains about 0.2 mM sulfate on average. Within freshwater systems, there is a range from 0 to 2.4 mM in groundwater systems, from 0.02 to 2.6 mM in lakes, and from 0 to 6.6 mM in rivers (Guidelines for drinking-water quality: recommendations, 2004). Based on the energetic yield for microbial biogeochemical reactions, microbial metabolisms follow a predictable sequence (referred to as the classic redox tower or thermodynamic ladder) of terminal electron acceptors (Champ et al., 1979). It is assumed that microbial respiration of Fe(III) is more prominent than that of sulfate in all aquatic systems except those with high sulfate concentrations (Froelich et al., 1979; Hoehler et al., 1998; Lovley and Phillips, 1987; Patrick and Henderson, 1981). Thus, researchers broadly follow the thermodynamic predictions and postulate that microbial Fe(III) respiration is expected to outcompete sulfate, and hence that sulfate reduction is a minor controlling factor on Fe reduction in freshwater systems that are usually associated with low sulfate levels (Hansel et al., 2015).

As the dominant ferric Fe species in natural systems, Fe oxides have a range of crystallinity. By calculating the Gibbs free energy (ΔG), Postma and Jakobsen (1996) predicted that the reduction of sulfate is more favorable than reduction of more crystalline Fe oxides, such as goethite and hematite, but less energetically favorable than amorphous and highly reactive Fe oxides, such as ferrihydrite (HFO). Researchers have confirmed experimentally that the reduction of more crystalline Fe oxides either coincides with or precedes sulfate reduction under most

environmentally relevant settings (Bethke et al., 2011; Jakobsen & Postma, 1999; Postma & Jakobsen, 1996; Williams et al., 2011). The total energy cannot be simplified as representing the metabolically usable energy, and the energy budget incorporating the relevant mineralogical structure should be used as the metabolic predictor (Bethke et al., 2011; Jakobsen & Postma, 1999; Postma & Jakobsen, 1996; Williams et al., 2011). Previous observations showed that active and sustained sulfur cycling can occur in low-sulfate natural environments either in the absence of Fe oxides or in the presence of highly crystalline Fe oxides. This occurs because Fe(III) hosted in the highly crystalline Fe oxides aids with the cycling and regeneration of sulfate and intermediate sulfur species, but amorphous HFO will be consumed before sulfate (Holmkvist et al., 2011; Pester et al., 2012).

Recently, Hansel et al. (2015) published a systematic investigation that determined how sulfate affected microbial Fe oxides reduction in natural freshwater systems. Natural freshwater sediments (collected from Ashumet Pond, Falmouth, MA, USA) mixed with Al-substituted ferrihydrite, two-line ferrihydrite, goethite or hematite-coated quartz sands were used in flow-through experiments (Table 1). An artificial groundwater media was pumped through the column at 0.2 m/day within the natural groundwater flow rate (Hansel et al., 2015).

Table 1. Geochemical analyses of flow-through experiments (modified from Hansel et al., 2015).

		Control	Ferrihydrite	Al-ferrihydrite	Goethite	Hematite	
 Flow	Influent (μmol)	Sulfate	205	248	223	219	200
	Solid phases (μmol)	Sulfide (in)	1	119	145	134	132
		Fe(II) (in)	1	652	648	231	221
		Sulfide (out)	3	1	2	4	0
		Fe(II) (out)	2	563	787	18	50
	Effluent (μmol)	Sulfate	2	2	2	3	2
		Sulfide(aq)	165	1	1	8	3
		Fe(II) _{aq}	1	208	135	38	33

Using influent and effluent aqueous concentrations, the useable energy (ΔG) was calculated as shown in Table 2. The reduction of HFO had a much larger ΔG than the reduction of sulfate, which is consistent with previous findings that HFO reduction occurs before sulfate reduction (Bethke et al., 2011; Jakobsen and Postma, 1999; Postma and Jakobsen, 1996; Williams et al.,

2011). However, within the columns containing goethite and hematite, and the columns containing Al-substituted ferrihydrite and two-line ferrihydrite, sulfate was fully consumed rapidly via reduction to sulfide (Table 1). Combining the solid-phase distribution patterns (Table 1) with microbial respiratory sequence analysis (Figure 1), Hansel et al. (2015) inferred that sulfate-reducing bacteria dominated the microbial communities along the beginning of the flow path. In contrast, Fe-reducing bacteria dominated down-gradient, that is, for HFO, dissimilatory Fe reduction became dominant only after sulfate reduction ended. This finding overturned the previous thinking by Postma and Jakobsen (1996). Based on the predicted abiotic FeS reactions, it can be assumed that each mole of biogenic sulfide reacts with HFO to produce two moles of Fe(II) (Table 2), but the ratios of Fe(II) to sulfide are in excess of 2. In addition, no known Fe-reducing bacterium was observed within the hematite and goethite columns and the bottom of the HFO columns (Table 1). Thus, other ferrous Fe sources may exist.

Table 2. Gibbs free energy for reduction of Fe(III) and sulfate (modified from Hansel et al., 2015).

	ΔG (kJ/mol ATP)
Metabolic reactions:	
(1) $C_6H_5O_2^- + 4Fe(OH)_3 + 7H^+ \rightarrow C_2H_3O_2^- + HCO_3^- + 4Fe^{2+} + 10H_2O$	257
(2) $C_2H_3O_2^- + 8Fe(OH)_3 + 15H^+ \rightarrow 2HCO_3^- + 8Fe^{2+} + 20H_2O$	425
(3) $C_3H_5O_3^- + 4FeOOH + 7H^+ \rightarrow C_2H_3O_2^- + HCO_3^- + 4Fe^{2+} + 6H_2O$	174
(4) $C_2H_3O_2^- + 8FeOOH + 15H^+ \rightarrow 2HCO_3^- + 8Fe^{2+} + 12H_2O$	258
(5) $C_3H_5O_3^- + 0.5SO_4^{2-} \rightarrow C_2H_3O_2^- + HCO_3^- + 0.5HS^- + 0.5H^+$	60
(6) $C_2H_3O_2^- + SO_4^{2-} \rightarrow 2HCO_3^- + HS^-$	57
(7) $C_3H_5O_3^- + 2S^0 + 2H_2O \rightarrow 2HS^- + HCO_3^- + C_2H_3O_2^- + 3H^+$	N/A
(8) $C_2H_3O_2^- + 4S^0 + 4H_2O \rightarrow 4HS^- + 2HCO_3^- + 5H^+$	N/A
Predicted abiotic FeS reactions:	
(9) $HS^- + 2Fe(OH)_3 + 5H^+ \rightarrow 2Fe^{2+} + S^0 + H_2O$	N/A
(10) $HS^- + 2FeOOH + 5H^+ \rightarrow 2Fe^{2+} + S^0 + 4H_2O$	N/A
(11) $Fe^{2+} + HS^- \rightarrow FeS + H^+$	N/A

***Note: N/A means not available. ΔG means the usable energy. Higher ΔG means the reaction is more favourable.**

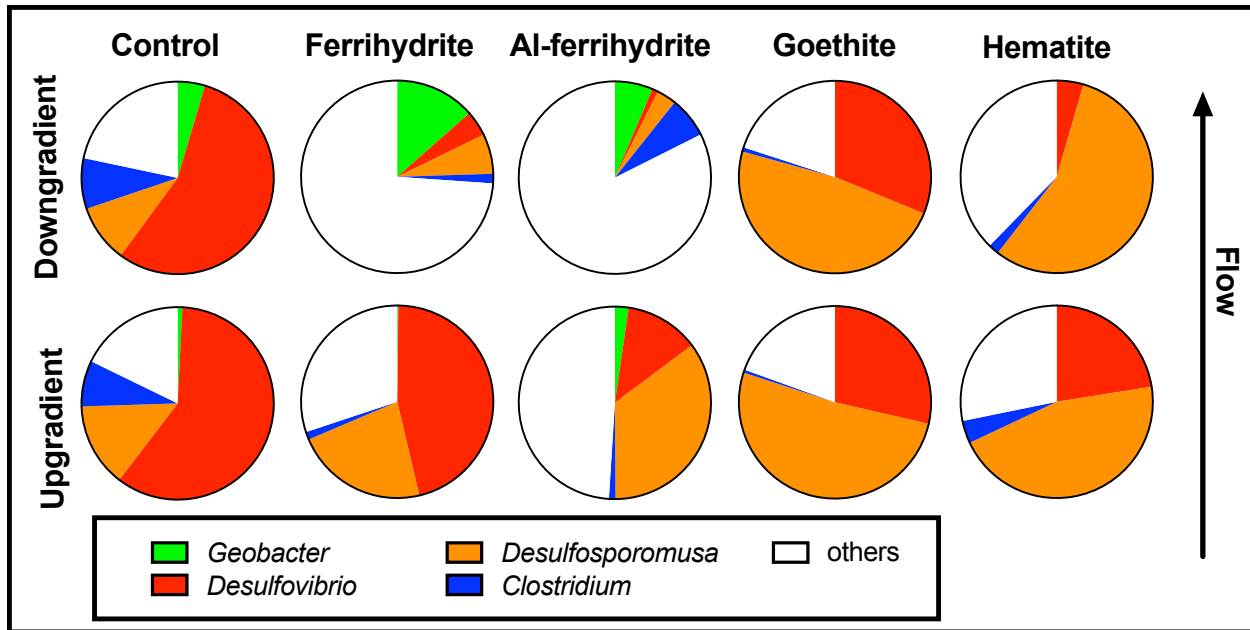


Figure 1. Microbial respiratory sequences with the sediments collected from Ashumet Pond, Falmouth, MA, USA (modified from Hansel et al., 2015). The only known dissimilatory iron-reducing bacterium observed was *Geobacter*. The sulfate-reducing organisms observed were *Desulfovibrio* and *Desulfosporomusa*, and both of these bacterial strains can enzymatically reduce Fe. The only known iron-reducing fermenter observed was *Clostridia* (Dobbin et al., 1999, Dominik et al., 2002). The potential for Fe reduction by other bacteria is not known.

Hansel et al. (2015) made a schematic diagram to show the cumulative fluxes of different chemical species in the flow-through column (Figure 2). A cryptic sulfur cycle (sulfide oxidation and the subsequent re-reduction of intermediate elemental sulfur) was observed, similar to that observed in some high-sulfate settings such as marine and subglacial environments (Holmkvist et al., 2011; Mikucki et al., 2009). The relative importance of S recycling in catalyzing HFO reduction was calculated (Figure 2). About 51% of the sulfide reacted with HFO to form elemental sulfur (S^0) whereas the remaining 49% of sulfide combined with Fe(II) and precipitated as FeS. A majority of the S^0 (equivalent to 40% of the original sulfate) was re-reduced to sulfide, whereas the remainder (equivalent to 11% of the original sulfate) stayed as S^0 in this system. Because of this cryptic sulfur cycle, about 30% Fe(II) within the HFO column can be explained by the additional Fe(III) reduction caused by sulfide oxidation and the subsequent re-reduction of intermediate elemental sulfur. Nearly 39% of the observed Fe(III) reduction can be explained by the reaction of biogenic sulfide and HFO. The remaining 31% of Fe(III) reduction was caused by

microbial Fe respiration. Therefore, the findings of Hansel et al. (2015) posed a challenge to conventional wisdom and suggested that sulfur cycling could be a significant driver of Fe cycling in low-sulfate conditions regardless of the crystallinity of the Fe oxides.

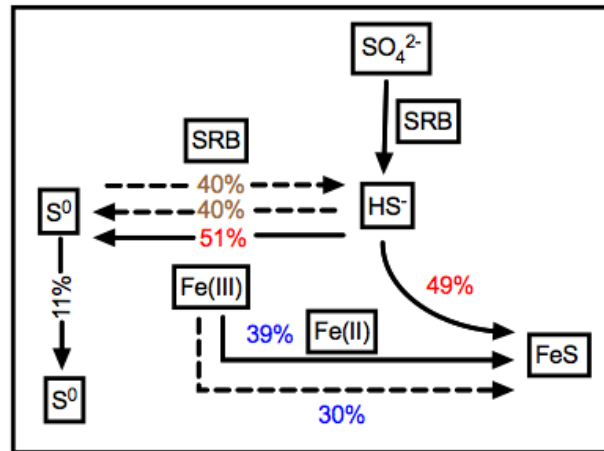


Figure 2. Cryptic S cycle during Fe(III) reduction (modified from Hansel et al., 2015). Numbers in blue indicate 39% of Fe(III) was reduced by sulfide derived from sulfate reduction (solid lines) whereas 30% Fe(III) was reduced by sulfide derived from S⁰ reduction (dashed lines). The remaining 31% (i.e., 100 - 39 - 30) of the Fe(III) reduction was caused by the microbial Fe respiration. Numbers in black, red and brown reflect mass fluxes normalized to the amount of sulfate reduced. Numbers in red indicate that about 49% of the sulfide precipitated with Fe(II) as FeS, whereas about 51% of the sulfide reduced HFO and formed elemental sulfur (S⁰). Numbers in brown indicate that a total of 40% sulfate was involved in S recycling while 11% (i.e., 51 - 40) sulfate was reduced and remained as S⁰ in this system.

Although S was suggested to be more important than previously thought during Fe cycling in freshwater systems, the mechanism of these processes has not been well studied. The objective of this study is to first confirm the existence of the cryptic S cycle under low S conditions, and then use ferrihydrite (HFO), the most common substrate in natural environments (Tangalos et al., 2010), as the model Fe(III) mineral to investigate the extent of Fe(III) reduction and Fe isotope fractionations during: 1) nonenzymatic reduction of Fe(III) by sulfide generated by SRB (*D. vulgaris*); and 2) direct enzymatic reduction of Fe(III) by SRB (*D. vulgaris*). The results will be compared to determine if Fe isotopes can be used to distinguish between the two processes.

The first evidence for a connection between sulfate-reducing bacteria (SRB) and anaerobic Fe reduction was recognized more than a century ago (Enning & Garrelfs, 2014). Since then, scientific interest in the relationship between SRB and microbial Fe(III) reduction has increased tremendously. The potential for SRB to enzymatically reduce Fe(III) was studied. It was found that most SRB can enzymatically reduce Fe(III), but a few strains cannot (Lovley et al., 1993). This study will investigate two strains, *Desulfovibrio vulgaris*, which is usually found in freshwater systems and is capable of reducing chelated Fe(III) as well as insoluble Fe(III) oxides enzymatically, and *Desulfobacter curvatus*, which is usually found in marine systems and cannot enzymatically reduce Fe(III) (Lovley et al., 1993).

Known as a powerful tool to trace Fe redox processes in both modern and ancient environments (Johnson et al., 2008), Fe isotopes have been applied to infer biogeochemical conditions and processes in different systems, such as soils, rivers, lakes, groundwaters, and marine settings (Bergquist & Boyle, 2006; Fehr et al., 2008; Liu et al. 2015; Teutsch et al., 2005; Wiederhold et al., 2007). Both biotic and abiotic processes can fractionate Fe isotopes (Beard et al., 1999; Crosby et al., 2005; Crosby et al., 2007; Johnson et al., 2002; Johnson et al., 2005; Welch et al., 2003; Wu et al., 2011) and the largest fractionations are associated with redox changes (Johnson et al., 2008). Despite the importance of Fe reduction by sulfide, little is known about Fe isotope partitioning during this process as well as during enzymatic reduction of Fe minerals by SRB. The same Fe isotope fractionations are expected for enzymatically produced sulfide by two strains (*D. vulgaris* and *D. curvatus*) due to similar redox changes. However, the kinetics of the system may differ as a result of different pathways (i.e., Fe reduction by sulfide vs. enzymatically by SRB).

This study is important because, although sulfur cycling has been proposed to be more important for Fe cycling under low-sulfate conditions than previously thought (Hansel et al., 2015), the mechanism of SRB-induced Fe(III) reduction is not well understood (Enning & Garrelfs, 2014). Application of Fe isotope geochemistry to microbial Fe(III) reduction in low-sulfate environments is a novel approach that could shed light on the electron transfer and atom exchange pathways. Comparison of the Fe isotope data from this study (for nonenzymatic Fe(III) reduction by H₂S generated by SRB, and direct enzymatic Fe(III) reduction by SRB) with

previous studies on Fe(III) reduction by dissimilatory iron reducing bacteria (DIRB) allows an evaluation of Fe isotopes as a tracer for different pathways of Fe reduction in freshwater systems.

2.0 Background

2.1 Fe isotopes

Iron isotopes are valuable tools for analyzing Fe redox processes in modern and ancient environments (Beard et al., 1999; Crosby et al., 2007; Dauphas et al., 2017; Johnson et al., 2008). It has been shown that Fe isotopes have potential to be used for determining the relative contribution of different isotope fractionation pathways (e.g., Czaja et al., 2010; Czaja et al., 2012; Guilbaud et al., 2010; Heimann et al., 2010; Johnson et al., 2013; Rouxel et al., 2005; Rouxel et al., 2008). Both biotic and abiotic processes can fractionate Fe isotopes (Crosby et al., 2005), resulting in a large range of Fe isotope compositions in natural environments (Table 3). For example, it has been confirmed that in abiotic systems, Fe isotopes can be fractionated by ion-exchange (Anbar et al., 2000; Roe et al., 2003), and the abiotic precipitation of ferric oxides (Bullen et al., 2001; Skulan et al., 2002). By investigating the metabolic processing of Fe, previous studies have showed that organic ligands during mineral dissolution (Brantley et al., 2001), anaerobic photosynthetic Fe(II) oxidation (Croal et al., 2003), and dissimilatory iron reduction (DIR) by bacteria can all cause Fe isotope fractionation (Beard et al., 1999; Beard et al., 2003; Johnson et al., 2005). Beard et al. (2003) and Johnson et al. (2004) showed that the contribution of abiotic and biotic Fe redox cycling pathways to sediment diagenesis could be evaluated by analyzing the Fe isotope composition of sedimentary rocks.

The largest Fe isotope fractionations tend to occur between Fe(II) and Fe(III) in solution during redox and bonding changes in the natural environment that affect a portion of the Fe reservoir (Johnson et al., 2008). Different pathways of DIR of Fe(III) minerals such as goethite, hematite and ferrihydrite have been studied (e.g., Crosby et al., 2005; Lovley, 1987; Nealson and Myers, 1990). Although Fe isotope fractionation during sulfide-mediated HFO reduction in marine systems has been evaluated by previous studies (Canfield et al., 1992; Johnson et al., 2008; Severmann et al., 2006), no experimental Fe isotope studies have explored the different contributions of abiotic and biotic Fe redox cycling pathways during SRB-mediated reduction of HFO in freshwater systems. In this study, Fe isotopes are used as a tracer in laboratory experiments to analyze the mechanism of SRB-induced microbial Fe reduction under conditions mimicking a freshwater system with a low-sulfate concentration.

Table 3. Fe isotope compositions in natural environments.

Environments		$\delta^{56}\text{Fe}$ (‰)	Reference		
Rock record	Igneous rocks and oxic clastic sediments (loess, turbites)	~0	Huang et al., 2011; Poitrasson et al., 2013; Teng et al., 2011.		
	Anoxic clastic sediments (black shale)	-3.50 to +2.20	Jenkyns et al., 2007; Marin-Carbonne et al., 2014.		
	Chemically precipitated sediments (BIFs and Mn-Fe crusts)	-2.70 to +2.60	Craddock & Dauphas, 2011; Li et al., 2015; Planavsky et al., 2012; Raye et al., 2015; Steinhofel et al., 2010; Tsikos et al., 2010; Whitehouse & Fedo, 2007.		
Modern environment	Soils	-0.60 to +0.41	Guelke et al., 2010; Mansfeldt et al., 2012; Song et al., 2011.		
		Groundwater	-3.40 to +0.58	Guo et al., 2013; Teutsch et al., 2005.	
	Aquifers	Sediment	-1.10 to +0.75	Dekov et al., 2014; Guo et al., 2013; Teutsch et al., 2005; Xie et al., 2013; Xie et al., 2014.	
		Pore water	-1.81 to +0.64	Busigny et al., 2014; Percak-Dennett et al., 2013.	
	Terrestrial	Lakes	Sediment	-0.72 to +0.34	Busigny et al., 2014; Malinovsky et al., 2005; Percak-Dennett et al., 2013.
		Water column	-2.14 to +0.57	Busigny et al., 2014; Malinovsky et al., 2005; Percak-Dennett et al., 2013; Teutsch et al., 2009.	
	Rivers	Dissolved Fe	-0.60 to +0.51	Bergquist and boyle, 2006; Chen et al., 2014; Escoube et al., 2009	
		Suspended Fe	-0.90 to +0.31	Bergquist and boyle, 2006; Chen et al., 2014; Escoube et al., 2009; Ingri et al., 2006; Pinheiro et al., 2014.	
		Pore water	-4.00 to +1.22	Homoky et al., 2009; Homoky et al., 2013; Severmann et al., 2010.	
	Continental shelf	Sediment	-0.89 to +0.15	John et al., 2012; Scholz et al., 2014; Severmann et al., 2008; Severmann et al., 2010; Staubwasser et al., 2006.	
		Water column	-3.45 to +0.04	Chever et al., 2015; John et al., 2012.	
	Marine system	Seawater	-0.90 to +0.71	Gelting et al., 2010; Labatut et al., 2014; Radic et al., 2011; Rouxel & Auro, 2010.	
		Sediment	-1.80 to +1.00	Gelting et al., 2010; Conway & John, 2015; Fehr et al., 2010; Homoky et al., 2009; John & Adkins, 2012; Labatut et al., 2014; Moeller et al., 2014; Nishizawa et al., 2010.	

2.2 Desulfovibrio vulgaris & Desulfobacter curvatus

Dissimilatory SRB are one of the most ancient microbial forms of life on Earth, and its metabolic activity can be traced back more than three billion years by sulfur isotope evidence from the rock record (Widdel & Pfennig, 1981). A relatively wide range of genera of dissimilatory SRB has been identified (Widdel & Bak, 1992). Although SRB have a widespread occurrence in nearly all marine and terrestrial environments, distinctive from other types of bacteria, all known SRB are strict anaerobes. Hence, the pure cultures of these microorganisms not only require the absence of oxygen but also need a low redox potential of about zero to -100 mV (Alico & Liegey, 1966; Baas et al., 1955; Widdel & Pfennig, 1977).

Based on rRNA sequence analysis, SRB are divided into four groups: Gram-negative mesophilic SRB; Gram-positive spore-forming SRB; thermophilic bacterial SRB; and thermophilic archaeal SRB (Castro et al., 2000). Both *Desulfovibrio vulgaris* and *Desulfobacter curvatus* are Gram-negative mesophilic SRB. Two families of SRB are included in the gram-negative mesophilic SRB: the *Desulfovibrionaceae* and the *Desulfobacteriaceae*. *Desulfovibrio vulgaris*, which is capable of enzymatically reducing chelated Fe(III) and insoluble Fe(III) oxides, and is usually found in freshwater systems (Lovley et al., 1993), is a typical type of *Desulfovibrionaceae*. Cells of *Desulfovibrio* species are usually motile and curved (Widdel & Bak, 1992). The most commonly utilized organic substrates for this kind of SRB are lactate, acetate, ethanol, pyruvate, and fumarate, whereas H₂, acetate, and lactate are commonly used as electron donors (Widdel & Bak, 1992). *Desulfobacter curvatus*, which cannot enzymatically reduce Fe(III) and is usually found in marine systems (Lovley et al., 1993), is one of the *Desulfobacteriaceae* and usually has an oval shape (Widdel & Bak, 1992). The most characteristic and common electron donor for this kind of SRB is acetate.

3.0 Methodology

3.1 Experimental designs

In this study, Si-HFO coprecipitate was used instead of pure HFO since previous studies have shown that HFO, the most reactive Fe oxide, forms simply by Fe(II) oxidation or Fe(III) hydrolysis. However, HFO is metastable and can easily transfer to more stable and crystalline phases, such as goethite and hematite by dehydration and structural rearrangement (Jambor & Dutrizac, 1998). It has been shown that in the presence of some electron donors, such as Fe(II), the transformation of HFO into goethite, magnetite, and lepidocrocite will be greatly enhanced (e.g., Boland et al., 2013; Boland et al., 2014; Hansel et al., 2005). A more recent study pointed out that coexisting Si can influence the HFO transformation rate by inhibiting the precipitation of goethite and lepidocrocite, and promoting the precipitation of poorly crystalline ferrihydrite (Wang et al., 2015). Furthermore, when the concentration of Si increases, the intensity of the bond between HFO and Si increases. When the Si/Fe ratio becomes 5.8% to 27%, the transformation of HFO into goethite and lepidocrocite is almost completely inhibited (Wang et al., 2015). Thus, to keep HFO more stable, Si-HFO co-precipitates were synthesized by rapidly adding FeCl₃ solution into the Na₂SiO₃ solution with an equal molarity of dissolved Si, and 1 M NaOH was used to adjust the pH to around 7 (Wu et al., 2011).

The growth medium was centrifuged after the SRB had reached the mid- to late-log phase of growth (Liu et al., 2012). The enzymatically produced sulfide was prepared by filtering and collecting the aqueous phase of the growth medium. After the S concentration of this solution was measured, the enzymatically produced sulfide solution was sealed in the glove box and kept out of light for later use (this solution can only be stored for a few days). Cells of either *D. curvatus* or *D. vulgaris* were washed twice with a sterilized and anoxic 10 mM HEPES buffer in the glove box. The washed cells were dissolved in an appropriate amount of 10 mM HEPES buffer to make the final cell concentration approximately 1.5×10^8 cells/ml for both SRB strains. Subsequently, the solution was poured into 160 ml serum glass bottles and sealed with 20 mm blue stoppers and aluminum caps. As for the cultivation processes, all solutions and cultures were transferred via the gas distribution system using a N₂ : CO₂ ratio of 80 : 20 and purged sterilized syringes and needles. All bottles were incubated at 30 °C in the dark.

To investigate the extent of Fe(III) reduction and magnitude of Fe isotope fractionation during Fe(III) reduction enzymatically by SRB and non-enzymatically by SRB-generated sulfide, seven sets of experiments were conducted in this study (Table 4). In set 1, a total amount of 0.2 mM sulfide and 3.2 mM silicate and ferrihydrite co-precipitates (Si-HFO) were added without any SRB, which meant that Si-HFO could be directly reduced only by sulfide in this system. Thus, set 1 was considered as an abiotic control to examine the effect of abiotic Fe(III) reduction. In sets 2 and 4, SRB, 10 mM HEPES buffer, 3.2 mM sodium acetate (for *D. curvatus*) or sodium lactate (for *D. vulgaris*), and 3.2 mM Si-HFO were mixed. Since Fe(III) can be enzymatically reduced by *D. vulgaris* but not by *D. curvatus* (Lovley et al., 1993), Fe(II) was expected to be produced in set 4, but not in set 2. These two sets were used to determine if the cultivated SRB were capable of enzymatically reducing Fe without a S source, and to identify the impact of SRB in biotic Fe(III) reduction. In sets 3 and 5, SRB (either *D. vulgaris* or *D. curvatus*), 0.2 mM sulfate, and 3.2 mM Si-HFO were added. In both systems, Fe(III) can be reduced non-enzymatically by the sulfide produced by SRB, but only in set 5 can Fe(III) be reduced enzymatically by SRB. According to Hansel et al. (2015), the cryptic sulfur cycle is expected to exist in these two sets and to result in a larger extent of Fe(III) reduction than sets 1, 2, and 4, because of the additional Fe(III) reduction caused by sulfide oxidation and the subsequent re-reduction of intermediate elemental sulfur. In sets 6 and 7, a total of 3.2 mM Si-HFO and 0.2 mM enzymatically produced sulfide was added.

All seven sets were used to investigate the extent of Fe reduction non-enzymatically by SRB produced sulfide or enzymatically by SRB, but only sets 4 and 7 (*D. vulgaris*) were used to determine the isotope fractionation during Fe(III) reduction caused by SRB or enzymatically produced sulfide from SRB, respectively. In this study, to mimic natural freshwater systems, the bioreduction experiments were performed in a non-growth medium that used 10 mM HEPES buffer to maintain the pH. Either sodium acetate (for *D. curvatus*) or sodium lactate (for *D. vulgaris*) was added as the electron donor in those experimental sets with cells.

Table 4. Experimental Designs.

Experiment Set	SRB	Iron source	Sulfur source
Set 1	None	Si-HFO	Sulfide
Set 2	<i>Desulfobacter curvatus</i>	Si-HFO	None
Set 3	<i>Desulfobacter curvatus</i>	Si-HFO	Sulfate
Set 4	<i>Desulfovibrio vulgaris</i>	Si-HFO	None
Set 5	<i>Desulfovibrio vulgaris</i>	Si-HFO	Sulfate
Set 6	None	Si-HFO	Enzymatically produced sulfide (by <i>D. curvatus</i>)
Set 7	None	Si-HFO	Enzymatically produced sulfide (by <i>D. vulgaris</i>)

3.2 Source of organisms and culturing techniques

The potential for SRB to either enzymatically or non-enzymatically reduce Fe(III) has been investigated by previous studies (Lovley et al., 1993). Two strains of sulfate-reducing bacteria were chosen for this study. *Desulfobacter curvatus* ATCC43919, which cannot enzymatically reduce Fe(III), was purchased from American Type Culture Collection (ATCC), Rockville MD, USA. *Desulfovibrio vulgaris* ATCC29579, which can enzymatically reduce chelated Fe(III) and insoluble Fe(III) oxides, was a gift from Dr. Deng Liu (China University of Geosciences, Wuhan, China). The SRB strains were cultured under strict anaerobic conditions with a gaseous N₂/CO₂ ratio of 80:20 and a pH of 7 at 30 °C.

3.2.1 Growth media

Multiple types of growth medium have been employed for cultivation of SRB (Widdel & Bak, 1992). The optimum form and amount of nutrients, vitamins, trace minerals, salts, and electron donors for *D. curvatus* and *D. vulgaris* were modified in this study by lab experimentation and discussed in the following sections.

Prior to the bioreduction experiments, *D. curvatus* was cultured in an acetate medium, which was modified from ATCC medium 1648. In this medium, acetate serves as both an electron donor and carbon source, and Na₂SO₄ was used as an electron acceptor. The medium was buffered with NaHCO₃ and contained trace elements and vitamins. The *D. curvatus* medium consisted of 21.0 g NaCl, 3.0 g MgCl₂ x 6H₂O, 0.5 g KCl, 0.15 g CaCl₂ x 2H₂O, 0.3 g NH₄Cl, 0.2 g KH₂PO₄, 2.5 g sodium acetate, 3.0 g Na₂SO₄, 0.1 ml 0.5% resazurin, 2.5 g NaHCO₃, 1 ml trace element solution SL-10, and 10 ml Wolfe's vitamin solution. MilliQ water was added to bring the

total volume to 1000 ml. Trace-metal grade HCl was used to adjust the pH of the solution to around 7. The trace element solution consisted of 10 ml 25% HCl, 190 mg $\text{CoCl}_2 \times 6\text{H}_2\text{O}$, 100 mg $\text{MnCl}_2 \times 4\text{H}_2\text{O}$, 70 mg ZnCl_2 , 6 mg H_3BO_3 , 36 mg $\text{Na}_2\text{MoO}_4 \times 2\text{H}_2\text{O}$, 24 mg $\text{NiCl}_2 \times 6\text{H}_2\text{O}$, and 990 ml distilled water (Widdel et al., 1983). Wolfe's vitamin solution consisted of 2 mg biotin, 2 mg folic acid, 10 mg pyridoxine hydrochloride, 5 mg acidic thiamine, 5 mg riboflavin, 5 mg nicotinic acid, 5 mg calcium D-(+) – pantothenate (Na salt), 0.1 mg vitamin B_{12} , 5 mg p-aminobenzoic acid, 5 mg thiocetic acid, and 1000 ml MilliQ water.

D. vulgaris, as a common *Desulfovibrio* species, was cultured in a medium modified from a frequently used simple lactate medium (Widdel & Bak, 1992). In this medium, lactate was used as both an electron donor and carbon source, and Na_2SO_4 was used as an electron acceptor. The medium was buffered with KH_2PO_4 and instead of trace elements and vitamins, yeast extract was added. The *D. vulgaris* growth medium consisted of 1.0 g NH_4Cl , 0.5 g KH_2PO_4 , 1.08 g $\text{CaCl}_2 \times 2\text{H}_2\text{O}$, 1.648 g $\text{MgCl}_2 \times 6\text{H}_2\text{O}$, 1.0 g yeast extract, 0.1 ml 0.5% resazurin, 7.0 g 50% sodium lactate solution, 2.272 g Na_2SO_4 , and MilliQ water was added to bring the total volume to 1000 ml. NaOH was used to adjust the pH of the solution to around 7.

Since both *D. curvatus* and *D. vulgaris* are very sensitive to O_2 , it is necessary to maintain a strict anaerobic solution for their growth (Widdel & Bak, 1992). Therefore, resazurin was added to the *D. curvatus* and *D. vulgaris* media as a redox indicator to ensure that there is no O_2 in the system. In the growth medium, the color of the solution changes from blue to colorless as the O_2 content decreases (Figure 3). When the medium is colorless, it is considered to represent anaerobic conditions.

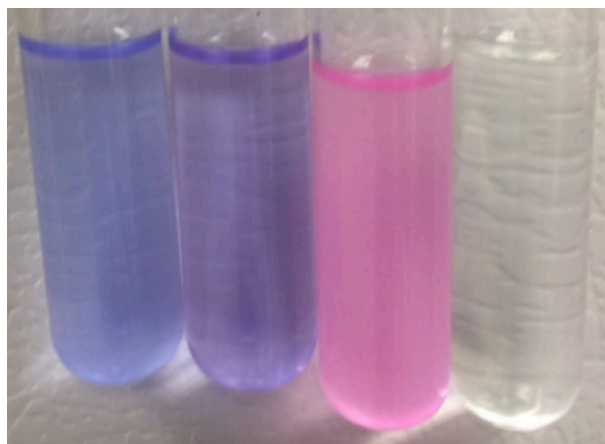


Figure 3. Color indicator for O₂ concentrations in growth mediums with resazurin. O₂ content decreases from the left to the right. Colorless growth medium is strictly anoxic.

To make sure that the growth medium is under anaerobic conditions, the medium is separated into glass tubes (9 ml for each medium), purged without caps for 6 min to remove the majority of O₂ content, and with caps for 6 min to remove the remaining small amount of O₂ content. The growth medium turned to light pink after being purged with the gas distribution system, which means almost all the O₂ was already removed. Subsequently, the growth medium was sealed with the aluminum cap, and autoclaved at 121 °C for 30 min using the liquid cycle. After autoclaving, 1 drop 0.17 M Na₂S solution is added into the glass tube to remove residual O₂ from the *D. curvatus* and *D. vulgaris* growth media. It usually takes > 2 hours for the Na₂S to completely react with the O₂ (i.e., the growth medium turns to colorless). To avoid precipitation, Fe is not included in the growth medium of both strains. The growth medium should be stored in the dark and at room temperature.

3.2.2 Cultivation techniques

To keep the growth medium fresh, either sodium acetate (*D. curvatus*) or sodium lactate (*D. vulgaris*) (as carbon source, energy source, and electron donor) and Na₂SO₄ (as electron acceptor) were added separately right before transferring the cells. The appropriate amount for *D. curvatus* was 0.15 ml 2 M sodium acetate and 0.10 ml 2 M Na₂SO₄ per 9 ml growth medium, whereas the appropriate amount for *D. vulgaris* was 0.10 ml 2 M sodium lactate and 0.08 ml 2 M Na₂SO₄ per 9 ml growth medium.

In case of rapid and robust growth, cells should be transferred using the gas distribution system or in the anaerobic glove box every few days by following the cell transfer protocol for *D. curvatus* and *D. vulgaris* (see Supplementary Information (SI)).

Once the cells have grown, frozen cultures should be prepared for the experiments. First, a healthy SRB culture was chosen once the optical density at 600 nm was slightly higher than 0.5 (Figure 4). Second, a deoxygenated preserving medium was prepared by adding 3 ml glycerol into 7 ml fresh growth medium. The biomass was concentrated by centrifugation in the anaerobic glove box at 8000 rpm for 10 min, and cells were re-suspended in the deoxygenated preserving medium. The cells and medium were mixed well, and then the culture was separated into 10 fisherbrand microcentrifuge tubes (2 ml) with screw cap o-rings and attachment loops (sterilized once) (1 ml of culture was used for each tube) within a clean bench. The tubes were sealed quickly and stored in a - 80 °C freezer.

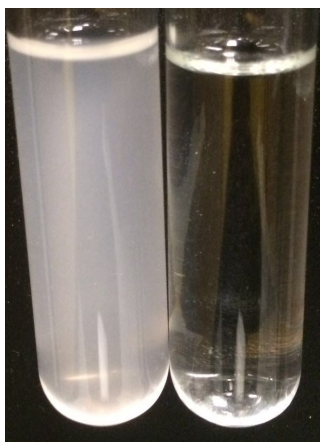


Figure 4. Growth cultures of *D. curvatus* with different optical density. Right tube indicates the original growth culture with an optical density near 0. Left tube indicates the growth culture with an optical density near 0.5 and is ready to transfer.

3.2.3 Cell counting

Cell counting is necessary to determine the quantity of cells. Since the cell counting process is complex, a growth curve (cell density versus optical density) is recommended here to streamline the experimental procedure and avoid having to do a cell count before each bioreduction experiment. To plot the growth curve, several cultures with different optical

densities (OD) were chosen first. Cell suspensions were taken from each culture and stained using acridine orange (AO) (see SI). After staining the cells, an epifluorescence microscope was used to count the cells. Using equation (1), the bacterial density of the original culture was determined.

$$\text{Bacteria Density/ml} = \frac{\text{Membrane conversion factor} \times \text{avg.no.of bacteria per net microscope field}}{\text{Dilution Factor}} \quad (1)$$

where

$$\text{Membrane conversion factor} = \frac{\text{Wet area of 25 mm membrane}}{\text{Area of microscope field}} \quad (2)$$

$$\text{Avg.no.of bacteria per net microscope field} = \frac{\text{Total number of bacteria counted}}{\text{Number of microscope fields counted}} \quad (3)$$

Thus, by comparing the cell and optical densities, the growth curve for either *D. curvatus* or *D. vulgaris* was plotted. Once the growth curves for these two bacteria were determined, the cell density of an unknown sample was calculated directly by comparison with the optical density. Furthermore, the volume of culture that should be added to achieve a target cell density was identified.

3.3 Standard curve preparation & elemental concentration measurement

3.3.1 Fe standard curve and measurement

According to the Beer-Lambert law, there is a linear relationship between the concentration of a substance and the absorbance. Thus, a standard curve can be used to quantitatively determine either Fe(II) or total Fe concentration (Stookey, 1970). To develop the Fe(II) or Fe(III) standard curve, a primary Fe standard solution was prepared by dissolving a known amount of FeCl₂·4H₂O or FeCl₃ in 0.5 M HCl in the glove box. The primary standard was diluted to a Fe concentration of 1000 μM. The suggested concentration range of the Fe calibration standards is from 0 to 1000 μM, as shown in Table 5.

Table 5. Suggested Fe concentration for Fe standard curve.

Standard	S9 (ml)	0.5 M HCl (ml)	Fe Concentration (μM)
Blank	0	5.00	0
S1	0.10	4.90	20
S2	0.25	4.75	50
S3	0.50	4.50	100
S4	0.75	4.25	150
S5	1.00	4.00	200
S6	1.50	3.50	300
S7	2.50	2.50	500
S8	3.50	1.50	700
S9	5.00	0	1000

***Note: S9 was prepared first, and then all the other standards were diluted from S9.**

The concentrations of Fe(II) and total Fe in each sample were measured spectrophotometrically by following a highly sensitive yet low-cost technique called the ferrozine method (Stookey, 1970; Viollier et al., 2000). The Fe(III) concentration was calculated by the difference between the Fe(II) and total Fe concentrations. Since only Fe(II) can react with ferrozine to form a stable complex species that is soluble in water between pH values of 4 and 9 (Figure 5), hydroxylamine hydrochloride was used as a reductant for Fe(III) in this method (Stookey, 1970). Previous spectrophotometric titrations have demonstrated that the ferrous complex of ferrozine has a single sharp peak at 562 nm for the maximum absorbance (Figure 6) (Stookey, 1970).

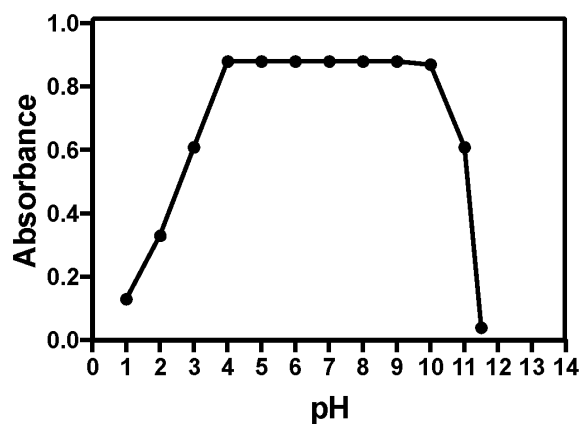


Figure 5. The effect of pH on the formation of the ferrous complex of ferrozine (modified from Stookey, 1970).

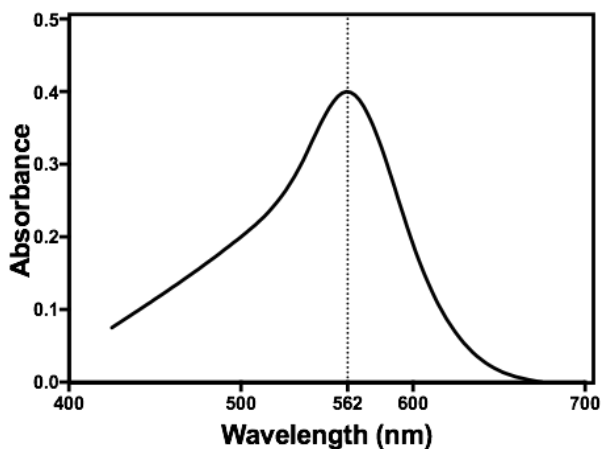


Figure 6. The visible absorption spectrum of the ferrous complex of ferrozine (a single sharp peak occurs at 562 nm) (modified from Stookey, 1970).

To determine the Fe(II) concentration, 1 ml 1 g/l ferrozine solution and 38 μ l Fe(II) standard solution were added to a 1 cm cell and measured immediately at 562 nm using a spectrophotometer (Viollier et al., 2000). Since the Fe(III) standard solutions needed to be reduced to Fe(II) before reacting with ferrozine, 1 ml 1 g/l ferrozine solution, 100 μ l 10% hydroxylamine hydrochloride, and 38 μ l standard solution were mixed first and measured > 6 hours later at 562 nm using a UV spectrophotometer to determine the total Fe concentration (Viollier et al., 2000). The blank reagent for Fe(tot) standard was prepared by mixing 100 μ l 10% hydroxylamine hydrochloride and 1 ml 0.5 M HCl solution. When calculating either Fe(II) or Fe(tot) concentration from the standard curve, the blank reagent needs to be subtracted from the sample absorbance (Viollier et al., 2000). The reproducibility of Fe spectrophotometric measurements in this study is within 5% except for samples with very low absorbance (< 0.05).

Once the concentration of Fe(II) and Fe(tot) were measured at selected time points (set 1: at starting point, 5 min, day 1, 3, 10, 20; sets 2, 3, 5: at starting point, day 1, 3, 5, 10, 15, 20; sets 4, 6, 7: at day 5, 8, 15, 20), the extent of Fe(III) reduction can be monitored. The extent of reduction was calculated using equation 4 for each time point (Liu et al., 2012).

$$\text{Reduction extent} = \frac{Fe(II)_{total} - Fe(II)_{initial}}{Fe(III)_{initial}} \times 100\% \quad (4)$$

The initial value is measured at the starting time point. The reduction capacity, which is the ultimate extent of Fe(III) reduction, is determined at the point when no more Fe(II) is produced (Liu et al., 2012). Typical standard curves developed in this study for Fe(II)/Fe(tot) (0-1000 μM) are shown in Figure 7.

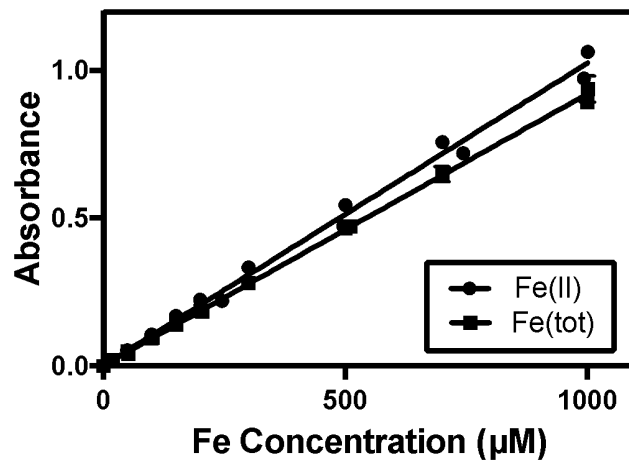


Figure 7. Fe(II) / Fe(tot) standard curves (at 562 nm).

3.3.2 S Standard curve and measurement

Similar to Fe, there is a linear relationship between the concentration of a substance and the absorbance for S (Cline, 1969). A colorimetric method called the methylene blue method can be used to quantitatively analyze dissolved hydrogen sulfide (H_2S , HS^- , S^{2-}) concentrations (Fischer, 1883; Cline, 1969). This method is applicable to natural waters with sulfide-sulfur concentrations ranging from 0 to 1000 μM , and over a salinity range of 0 to 40‰ (Cline, 1969). Cline (1969) showed that the slope of the S calibration curve is a function of the S concentration used (Figure 8). For example, the S calibration curve is much flatter for S concentrations lower than 1 μM compared with those for S concentrations higher than 1 μM .

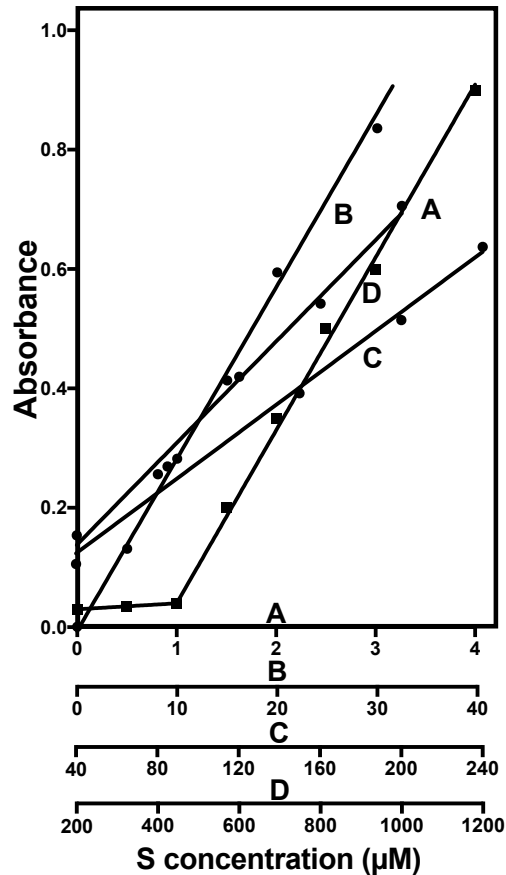


Figure 8. S calibration curves with different ranges of S concentration (modified from Cline, 1969).

To be more confident about the precision and accuracy of the measurement for the lower part of the standard curve, three different sets of S standard solutions were prepared in this study. The S concentrations of the standard solutions for high-S samples ranged from 0 to 50 μM , those for intermediate-S samples ranged from 1 to 4 μM , and those for low-S samples ranged from 0 to 0.4 μM (Table 6). All standard solutions were prepared in 0.25 M NaOH.

Table 6. Suggested S concentration intervals for sulfur standards with different S concentration ranges.

Standard Sulfur Concentration (μM)		
Sample S = 0-80	Sample S = 0-0.35	Sample S = 1-4
0	0	0
5	0.025	1
10	0.05	1.5
20	0.075	2
40	0.1	2.5
50	0.125	3
60	0.15	3.5
70	0.175	4
80	0.2	
	0.25	
	0.3	
	0.35	

To prepare the S standards, a sulfur stock solution was prepared first by dissolving 120 mg $\text{Na}_2\text{S}\cdot 9\text{H}_2\text{O}$ in 50 ml oxygen-free MilliQ water to make a final S concentration of 10 mM. Since the main sulfur stock solution is very sensitive to light and oxygen, it should be kept in the anaerobic glove box, protected from light, and prepared every few days (Cline, 1969).

The standard solutions with lower S content were prepared by diluting the sulfur stock solution with oxygen-free MilliQ water. Standard solutions with relatively low S concentrations should be used immediately after being prepared. Different colorimetric reagents and cuvettes (which caused different path lengths of UV light through the measured solutions) should be applied for the various sulfide-sulfur concentration ranges (Table 7) (Cline, 1969).

Table 7. Suggested reagent concentrations for sulfide-sulfur analysis for different sulfide concentrations (modified from Cline, 1969).

Sulfide concentration (μM)	Diamine solution concentration (g/500 ml)	Ferric solution concentration (g/500 ml)	Dilution factor (ml:ml)	Path length (cm)
1-3	0.5	0.75	1:1	10
3-40	2.0	3.0	1:1	1
40-250	8.0	12.0	2:25	1
250-1000	20.0	30.0	1:50	1

Colorimetric reagents for the UV measurement included solution A and solution B. Solution A was prepared by dissolving $\text{FeCl}_3\cdot 6\text{H}_2\text{O}$ in 6 M HCl, while solution B was prepared by

dissolving N, N-diméthyl-p-phenylenediamine sulfate in concentrated H₂SO₄. To efficiently remove the O₂ completely, every 160 ml of solution A and solution B should be purged with oxygen-free N₂ using a gas distribution system without cap for 30 min (quickly removes most O₂) and with cap for 30 min (completely removes any remaining O₂) before storage. Both solution A and solution B can be stored in the refrigerator at 4°C and protected from light by aluminum foil wrap for a long period (several months).

The same time point as Fe measurements was used for the S measurements. To use the methylene blue method to measure the concentration of sulfide, 0.4 ml solution A and 0.4 ml solution B were mixed thoroughly before sulfide solutions were added to them in the glove box (Cline, 1969). Solution A and solution B cannot be added separately because the apparent molar absorptivity would then be sensitive to temperature (Figure 9). The mixture of solution A and solution B reduced the volatilization of hydrogen sulfide and correspondingly increased the sensitivity of the measurement (Cline, 1969).

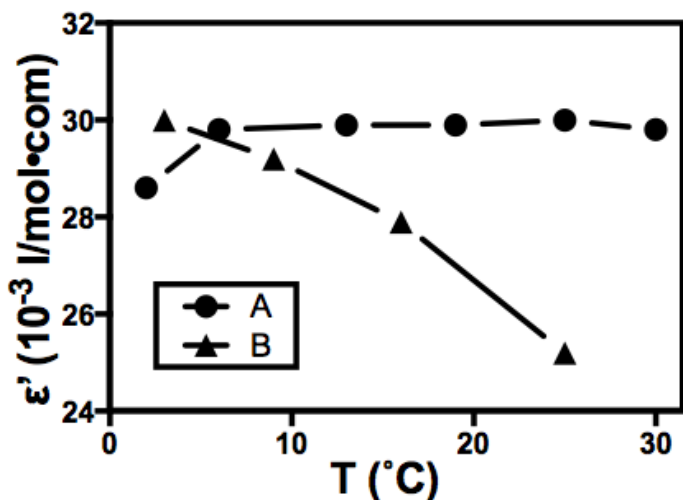


Figure 9. The effect of temperature on the colorimetric reagents (modified from Cline, 1969). Curve A shows the results when solution A and solution B were separately added into the sulfide solutions. Curve B shows the results when solution A and solution B were mixed thoroughly before sulfide solutions were added. The sensitivity of the method was defined in terms of the apparent molar absorptivity (ϵ').

After waiting about 30 min to ensure the color was stable, the mixture of sulfide solutions and colorimetric reagents was transferred to either a 1 cm UV cell (for the sulfide solutions with

S concentrations ranging from 0 to 50 μM), or a 10 cm cuvette (for the sulfide solutions with S concentrations ranging from 0 to 4 μM). The absorbance of samples was measured using the UV spectrophotometer at 670 nm and the sulfur concentration was calculated from the calibration curve. The reproducibility of S spectrophotometric measurements is within 5% in this study except for those samples with especially low absorbance (< 0.05). The typical standard curves developed in this study for sulfide at different concentration ranges (0 to 0.4 μM , 0 to 4 μM , 0 to 50 μM) are shown in Figure 10.

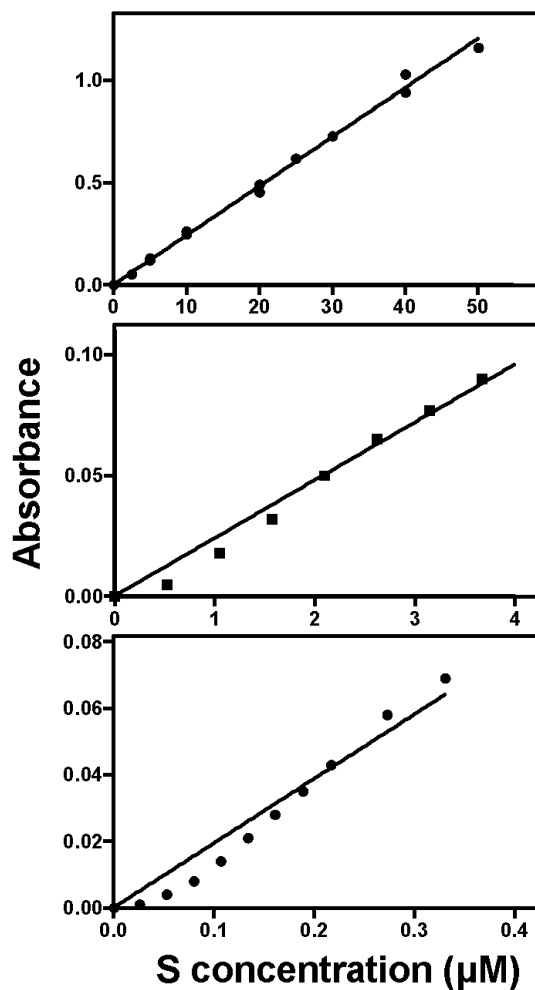


Figure 10. S standard curves for different S concentration ranges (measured at 815 nm). A 1 cm cuvette was used for the S standard curve ranging from 0 to 50 μM , whereas a 10 cm cuvette was used for the S standard curves ranging from 0 to 0.4 μM and 0 to 4 μM .

3.3.3 Si standard curve and measurement

Since Si-HFO co-precipitation was used in this study instead of HFO, the Si standard curve was also needed to ensure that an identical Fe:Si ratio of 1:1 was obtained for every Fe(III)–Si gel used. A Si concentration lower than 0.78 μM can be determined using the heteropoly blue method (Clesceri et al., 1989). A primary Si standard was prepared by dissolving $\text{Na}_2\text{SiO}_3 \cdot 9\text{H}_2\text{O}$ into MilliQ water to make a final concentration of around 6000 ppm. The primary Si standard was diluted using 0.5 M HCl to obtain a Si concentration of around 450 ppm. The Si calibration standard solutions were prepared using the second Si standard (450 ppm). A first set of more concentrated calibration standards were prepared by dilution with 0.5 M HCl, and they were stored for a relatively long time (several weeks). A second set of less concentrated Si calibration standards were prepared immediately prior to analysis by diluting the first set of calibration standards with MilliQ water (Table 8).

Table 8. Suggested Si concentrations for Si calibration standards.

Standard	Si concentration (ppm)	
	First Si calibration standards (with 0.5 M HCl)	Second Si calibration standards (with H_2O)
Blank	0	0
S1	5	0.15
S2	10	0.30
S3	15	0.45
S4	25	0.60
S5	45	0.75

For every 5 ml sample, 0.1 ml 6 M HCl and 0.2 ml ammonium molybdate reagent were added. To ensure a homogeneous solution, the mixture was inverted at least 6 times and allowed to stand for 5 to 10 min. Subsequently, 0.2 ml oxalic acid solution was added, mixed thoroughly, and allowed to stand for 2 to 15 min. Next, 0.2 ml ANSA (1-amino-2-naphthol-4-sulfonic acid) reducing agent was added, and mixed well. After 5 min, the color was photometrically measured. The color system obeys Beer's law at both 650 nm and 815 nm, but 650 nm has an appreciably reduced sensitivity (Clesceri, 1998). Thus, the absorbance was measured at 815 nm on the UV spectrophotometer in this study and the typical standard curves developed in this study for Si ranged from 0 to 0.75 ppm, and are shown in Figure 11. The reproducibility of Si

spectrophotometric measurements is within 5% in this study except for those samples with especially low absorbance (< 0.05).

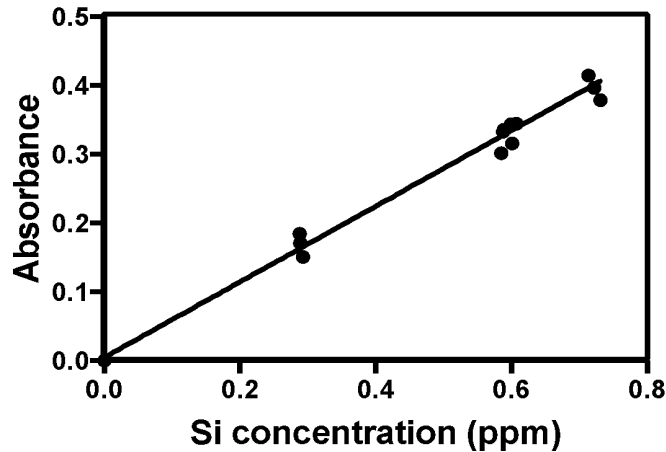


Figure 11. Si calibration standard curve (at 670 nm).

3.4 Sequential Fe extraction

To evaluate the extent of Fe(III) reduction via the Fe(II)/Fe(tot) ratio in different phases (aqueous, sorbed, and solid), 10 ml slurry was collected periodically from each bottle in the glove box. To separate the different Fe phases, a commonly performed method, the three-step sequential acid extraction (Figure 12), was used in this study. A bottle with 10 ml reaction slurry was first centrifuged at 8000 rpm for 20 min. After this step, aqueous Fe (Fe_{aq}) was collected by passing the supernatant through a 0.2 μ m pore size syringe filter. Subsequently, 10 ml 0.01 M HCl was added to the residual solid. After 10 min of reaction, the solution was centrifuged at 8000 rpm for 20 min, and the supernatant was filtered and collected as sorbed Fe (Fe_{sorb}). Next, 10 ml 0.5 M HCl was added to the residual solid. After 20 min, the solution was centrifuged at 8000 rpm for 20 min, and the supernatant was filtered to get the solid Fe (Fe_{solid}). In other studies, 7 M HCl was added after this step to get the crystalline Fe phases, such as magnetite, goethite and hematite (Wu et al., 2011; Liu et al., 2015). In this study, however, only the first three steps were performed since those crystalline Fe phases were not expected to form and almost all the remaining Fe was dissolved in 0.5 M HCl.

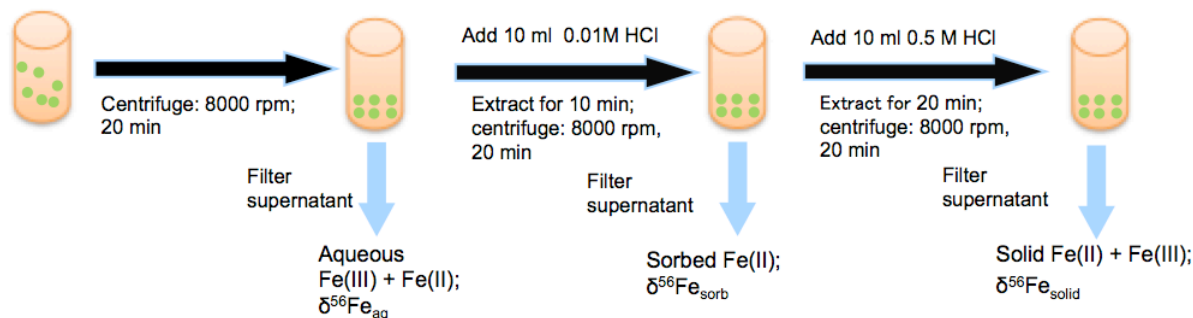


Figure 12. Three step sequential extraction of aqueous, sorbed, and solid Fe fractions.

After Fe phase separations, all extracts were acidified with 6 M HCl, and diluted to 0.5 M HCl in the anaerobic chamber (glove box) to avoid oxidation of Fe(II). The concentrations of Fe(II) and total Fe in each sample were measured spectrophotometrically by following the ferrozine method (Stookey, 1970; Viollier et al., 2000), and the Fe(III) concentration was calculated by the difference between Fe(II) and total Fe.

3.5 Fe isotope measurement

Prior to Fe isotope analysis, all samples were purified by anion-exchange chromatography following the procedures provided by Beard et al. (2003). To check the accuracy of the results, test solutions consisting of similar chemical compositions and a known Fe standard were prepared and measured. In this study, test solutions were prepared by adding HPS (high purity standard®) Fe (an in-house standard) to synthetic solutions, which included the same concentrations of major ions as the growth medium (Ca^{2+} , Mg^{2+} , K^+ , Na^+ , NH_4^+ , HCO_3^- , Cl^- , SO_4^{2-} , H_2PO_4^-), and which mimic those found in freshwater systems.

Preparation of samples for Fe isotope analysis was carried out in a metal-free clean room within the Metal Isotope Geochemistry Laboratory, University of Waterloo. All HCl used in this study was prepared by distilling reagent-grade HCl once through a Savillex DST-1000 acid distillation system. All HNO_3 used in this study was ultrapure HNO_3 (70% w/w, Omni Trace Ultra®). All Teflon beakers were pre-leached by adding 8 M HCl to each Teflon beaker (1 ml for 7 ml vials; 2 ml for 15-22 ml vials) and heated at 110°C for at least 8 hours before use. Samples with sufficient Fe (20-50 μg) were added to the Teflon beakers, and dried. Four drops ultra pure

HNO₃ were added to the sample and dried. This step was repeated twice. If samples contained organic matter, four drops H₂O₂ and 500 µl 7 M HCl were added and dried. Subsequently, 0.5 ml 7 M HCl was added and dried. The samples were preserved in closed Teflon beakers overnight or longer.

The anion-exchange columns were pre-leached with 1 ml ultrapure water twice. An appropriate amount of resin was loaded into the columns. The resin was rinsed twice with 800 µl 0.5 M HCl to remove all cations, and 800 µl 7 M HCl was passed through the column twice. A total of 100 µl 7M HCl was added to samples immediately prior to column chemistry. Samples were loaded onto the column and washed with 200 µl 7 M HCl. Subsequently, 600 µl 7 M HCl was passed twice through the resin to remove all cations except Fe. The Fe fraction was then collected in a new set of pre-leached Teflon beakers by passing 700 µl 0.5 M HCl three times through the resin. The samples were dried at 110°C on the hot plate and then re-dissolved in 100 µl 7 M HCl immediately prior to the second pass. Clean columns for the second pass were prepared in a similar manner as for the first pass. Samples were loaded, and 783 µl 7 M HCl was passed six times through the resin. The Fe fraction was then collected in a new set of pre-leached Teflon beakers by passing 700 µl 0.5 M HCl three times through the resin. A total of 38 µl of the collected Fe fraction was taken and used for ferrozine measurement to determine the post-column Fe concentration and compare with the Fe concentration before the column chemistry to make sure the yield was 100 ± 10%. The sample Fe fractions were dried and 4 drops ultra pure HNO₃ was added. Once all the Fe was dissolved, 4 drops H₂O₂ was added and then dried. These post-column chemistry steps were repeated twice. All samples (including test solutions and duplicates) were diluted in 2% HNO₃ to obtain a Fe concentration of 25 ppm for isotope analysis.

A multi-collector inductively coupled plasma mass spectrometry (MC-ICP-MS) method was used to precisely measure Fe isotope compositions. The MC-ICP-MS method provides a constant instrumental mass bias and a high ionization efficiency (Beard et al., 2003). In this study, Fe isotope compositions were analyzed using a Nu Plasma II MC-ICP-MS at the University of Wisconsin-Madison following established protocols (Beard et al., 2003; Severmann et al., 2006).

Isotopic compositions were reported as ⁵⁶Fe/⁵⁴Fe ratios using standard δ notation in units of per mil (‰):

$$\delta^{56}\text{Fe} = \left[\frac{{}^{56}\text{Fe}/{}^{54}\text{Fe}_{\text{sample}}}{{}^{56}\text{Fe}/{}^{54}\text{Fe}_{\text{std}}} - 1 \right] \times 10^3 \quad (5)$$

where ${}^{56}\text{Fe}/{}^{54}\text{Fe}_{\text{std}}$ is the average of the baseline for terrestrial igneous rocks ($\delta^{56}\text{Fe} = 0 \pm 0.05\text{‰}$ (Beard et al., 2003)).

The isotopic fractionation between two phases or species (A and B) was defined as:

$$\Delta^{56}\text{Fe}_{\text{A-B}} = \delta^{56}\text{Fe}_{\text{A}} - \delta^{56}\text{Fe}_{\text{B}} \quad (6)$$

Each individual sample solution was measured a total of 3 times and its 2SD was calculated. The 2SD for the samples were averaged to get an overall (mean) external precision for $\delta^{56}\text{Fe}$ of 0.08‰ (2σ ; $n=76$). The average $\delta^{56}\text{Fe}$ value of the test solutions was $0.09 \pm 0.08\text{‰}$ (2σ ; $n=12$), which is identical to the $\delta^{56}\text{Fe}$ measured for the pure HPS Fe solutions ($\delta^{56}\text{Fe} = 0.08 \pm 0.10\text{‰}$; 2σ ; $n=12$). The $\delta^{56}\text{Fe}$ of the IRMM-014 Fe isotope standard during the course of this study was $-0.08 \pm 0.10\text{‰}$ (2σ ; $n=13$), which lies within uncertainty of the long-term (several years) standard value of $-0.09 \pm 0.10\text{‰}$ (2σ ; $n > 100$) relative to average igneous rocks used in the lab at Wisconsin-Madison (Beard et al., 2003).

4.0 Results & Discussion

4.1 Growth curves for *Desulfobacter curvatus* & *Desulfovibrio vulgaris*

Following the method described in the cell counting section, sample pictures of the fluorescing *D. curvatus* and *D. vulgaris* cells under the epifluorescence microscope were observed as shown in Figure 13 and Figure 14. *D. curvatus* and *D. vulgaris* have similar size but different shapes. *D. curvatus* has a better absorptivity than *D. vulgaris*; thus, *D. curvatus* is more visible than *D. vulgaris* under the epifluorescence microscope. Growth curves for *D. curvatus* and *D. vulgaris* are shown in Figure 15 and Figure 16, respectively. A strong positive linear relationship was observed between the optical density (at 600 nm) and cell density for both *D. curvatus* ($R^2 = 0.999$) and *D. vulgaris* ($R^2 = 0.991$), and represents the bacterial growth curve.

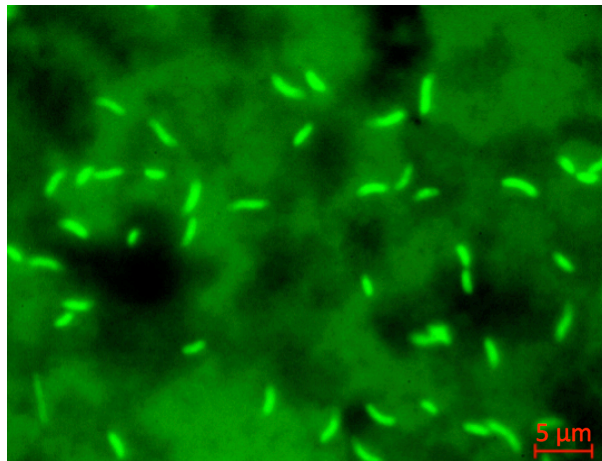


Figure 13. Sample picture of fluorescing *D. curvatus*.

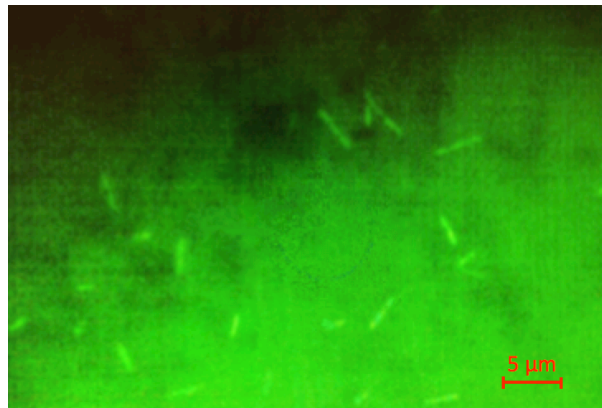


Figure 14. Sample picture of fluorescing *D. vulgaris*.

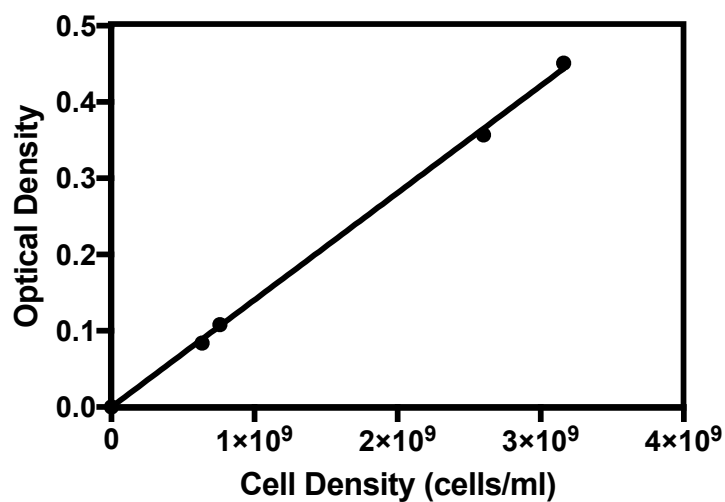


Figure 15. Growth curve for *D. curvatus*.

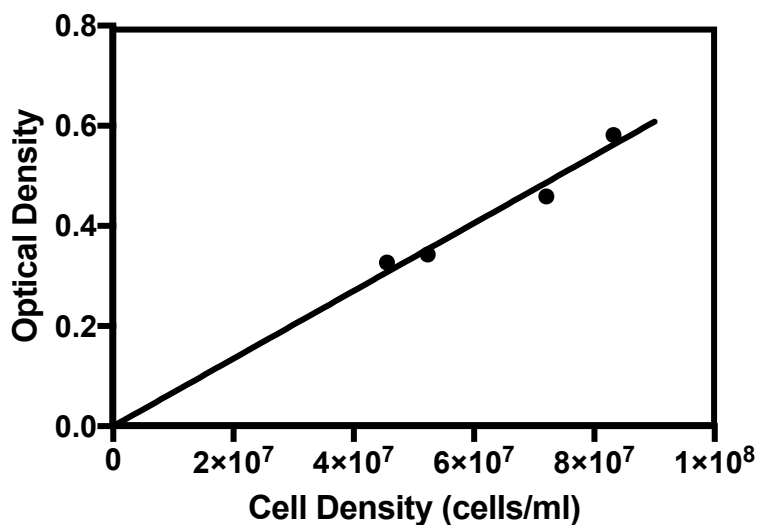


Figure 16. Growth curve for *D. vulgaris*

4.2 Elemental concentrations

Reagents in the abiotic experimental set 1 (0.2 mM Na₂S and 3.2 mM Si-HFO) reacted rapidly, and almost all the sulfide was consumed 5 min after Na₂S and Si-HFO were mixed in the glove box (Figure 17). A rotten-egg smell was detected at the end of this reaction, indicating the formation of H₂S. However, this amount of H₂S is not detectable, which means even a trace amount of H₂S will generate the smell. The Fe(II) concentration increased from 0 to around 400 μM (Figure 18) and stayed at this level for a relatively long time (20 days), which means that the

ratio between the concentration of generated Fe(II) and the initial sulfide concentration was around 2. This result is consistent with the previously predicted abiotic FeS reaction shown in Table 2 (Hansel et al., 2015).

D. curvatus and *D. vulgaris* were mixed with Si-HFO to detect their ability to reduce Fe in the absence of a S source. Fe(II) concentrations in all the phases were below the detection limit in the presence of *D. curvatus*, 3.2 mM Si-HFO, 3.2 mM Na-acetate, and 10 mM HEPES buffer, and the absence of sulfate (set 2). This result confirmed that the *D. curvatus* prepared in our lab does not have the ability to respire Si-HFO. By contrast, the existence of relatively low concentrations of Fe(II) (about 300 μ M) in the group with *D. vulgaris*, 3.2 mM Si-HFO, 3.2 mM Na-lactate, and 10 mM HEPES buffer (set 4) confirmed the ability of *D. vulgaris* to respire Si-HFO without any S source. However, the reaction rate in the group with *D. vulgaris* (set 4) was slower than the abiotic group (set 1) (Figure 18).

In experimental sets with SRB (set 3 with *D. curvatus* and set 5 with *D. vulgaris*), 0.2 mM Na₂SO₄ as a sulfate source, and 3.2 mM Si-HFO, sulfide concentrations slightly increased to around 5 μ M because of microbial respiration of Si-HFO. Subsequently, sulfide concentrations decreased and stayed at relatively low levels because of the consumption of Si-HFO (Figure 17). Slower reduction rates of HFO were detected in these sets compared with the abiotic set (Figure 18). The produced Fe(II) concentrations in both set 3 and 5 are higher than the total amount of produced Fe(II) concentration in set 1 and 4 (Figure 18) indicating the presence of a cryptic S cycle during sulfide-driven Si-HFO reduction mediated by either *D. vulgaris* or *D. curvatus* (Hansel et al., 2015).

The HFO reductions in the *D. curvatus* group were slightly slower than the *D. vulgaris* group (Figure 18), perhaps because *D. vulgaris* can enzymatically reduce Fe, but *D. curvatus* cannot (Liu et al., 2012; Lovley et al., 1993). However, no significant difference in Fe concentrations was observed between these two groups after the Fe concentration levelled off. This result showed that the reduction of HFO directly by *D. vulgaris* was minor. Hence, enzymatically produced sulfide was more important for microbial Fe(III) reduction, demonstrating that the cryptic S cycle is important for microbial Fe(III) reduction even at low levels of S (0.2 mM).

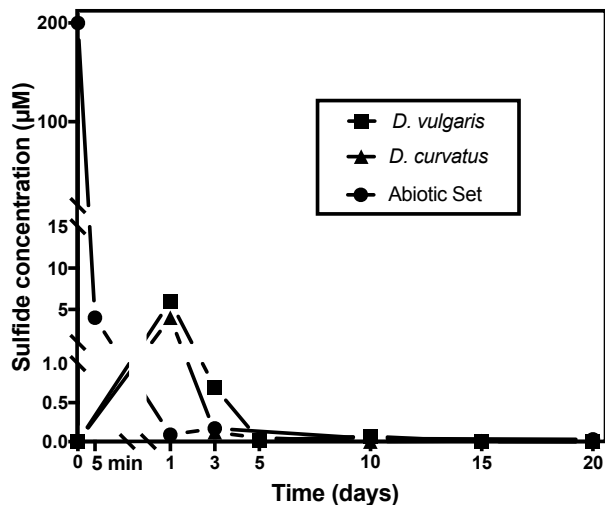


Figure 17. Changes in sulfide concentrations for different experimental sets (■ is set 5, ▲ is set 3, • is set 1; sulfide shown in this figure is the aggregate of sulfide in aqueous, sorbed, and solid phases).

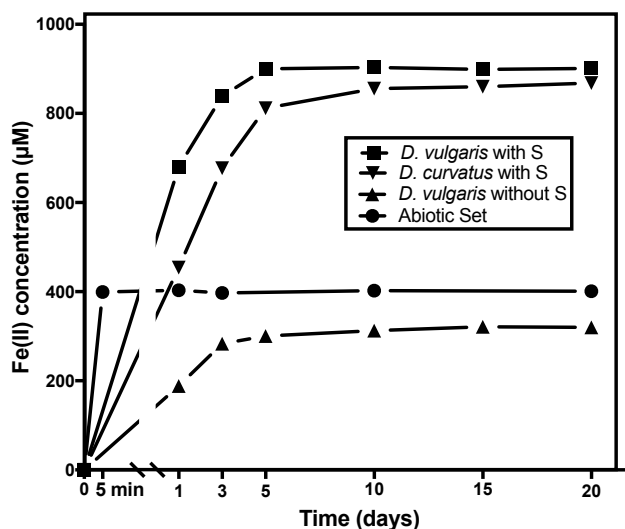


Figure 18. Fe(II) concentration over time in different experimental sets (■ is set 5, ▼ is set 3, • is set 1, ▲ is set 4; Fe(II) shown in this figure is the total amount of Fe(II) in aqueous, sorbed, and solid phases).

To further investigate the differences between Fe(III) reductions induced directly (enzymatically) by SRB and by sulfide produced by SRB, two experimental sets were performed: (1) 0.2 mM sulfide produced enzymatically by *D. vulgaris* or *D. curvatus*, and 3.2 mM Si-HFO (sets 6 and 7); and (2) *D. vulgaris*, 10 mM HEPES buffer, 3.2 mM sodium lactate and 3.2 mM Si-HFO (set 4). The extent of Fe(III) reduction was low (~10%) at a concentration of 3.2 mM Si-HFO (Figure 19). Different amounts of Si-HFO (0.7 mM and 10 mM) were used to examine

the effect on the extent of Fe(III) reduction. A higher concentration of Si-HFO does not increase the efficiency of Fe(III) reduction. The total amount of Fe(II) produced greatly depends on the initial amount of added sulfide (0.2 mM) or SRB (*D. vulgaris*). A similar amount of Fe(II) was generated with a different initial concentration of Si-HFO yet the same initial concentration of sulfide or *D. vulgaris*. Thus, a lower concentration of initial Si-HFO will cause a relatively higher extent of Fe(III) reduction.

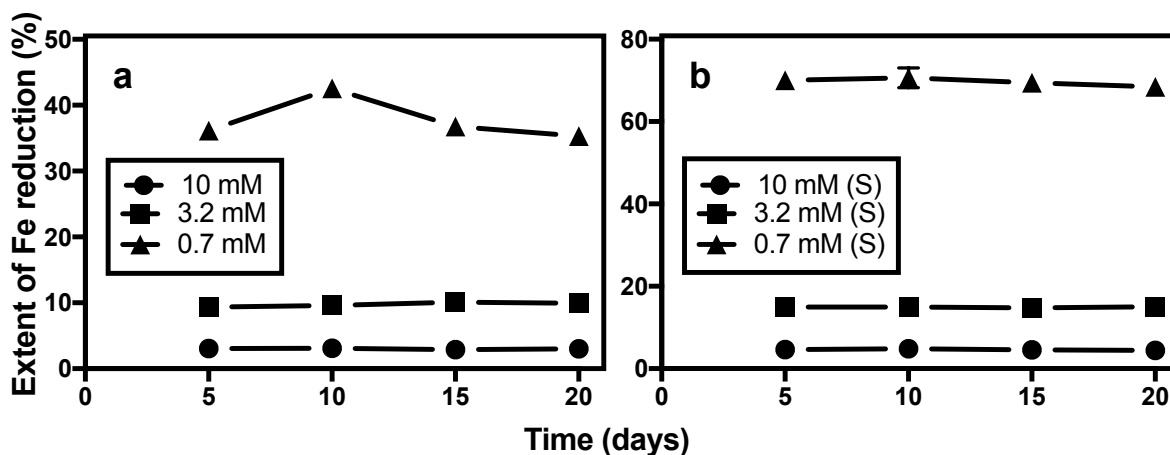


Figure 19. Extent of Fe(III) reduction by either *D. vulgaris* or the equivalent amount of sulfide produced by *D. vulgaris*, for different concentrations of Si-HFO. (a: *D. vulgaris*; b: *D. vulgaris* produced sulfide)

Based on these results, 0.2 mM enzymatically produced sulfide and a total amount of 0.7 mM Si-HFO were used to help investigate Fe reduction via different pathways (i.e., either induced directly by SRB or by enzymatically produced sulfide). Since the Si-HFO was diluted from a very concentrated Si-HFO gel, the total amount of Si-HFO used in each group was slightly different (Figure 20). Total Fe concentrations in all phases remained similar to the initial amount over time in each group, indicating that the loss of Fe during the entire experiments was negligible. In general, enzymatically produced sulfide resulted in a higher extent of Fe(III) reduction compared with direct Fe(III) reduction by SRB (*D. vulgaris*) (Figure 21). A significant difference in the extent of Fe(III) reduction was not observed using enzymatically produced sulfide from *D. vulgaris* versus *D. curvatus* (Figures 21 and 22). More specifically, the generated Fe(II) concentrations in both cases was around 450 μM , indicating that the ratio of Fe(II) produced to initial sulfide added was around 2.25. This ratio is similar to the abiotic experiment (set 1), suggesting that Fe respiration proceeded in a similar manner as abiotic Fe(III) reduction. The experiment with *D. vulgaris* without any S source (set 4) showed a relatively lower

concentration of Fe(II) (around 250 μM) than the abiotic set and the sets with enzymatically produced sulfide. Hence, the *D. vulgaris* cells have a relatively poor ability to reduce Fe(III) directly compared to sulfide. The extent of Fe(III) reduction in the sets with enzymatically produced sulfide remained nearly similar over time, whereas the extent of direct enzymatic Fe(III) reduction in the sets with cells increased and then slightly decreased over time. Since non-growth medium was used as matrix, and only sodium lactate and Si-HFO were applied as electron donor, electron acceptor, and nutrient in this group, it is not possible for *D. vulgaris* cells to stay alive for a long time. Thus, Fe(II) concentrations increased initially until the *D. vulgaris* cells died, after which time no more Fe(II) was produced. Since no significant loss of total Fe was detected, the slightly decreased Fe(II) concentration may be caused by the partial oxidation of Fe(II) to Fe(III).

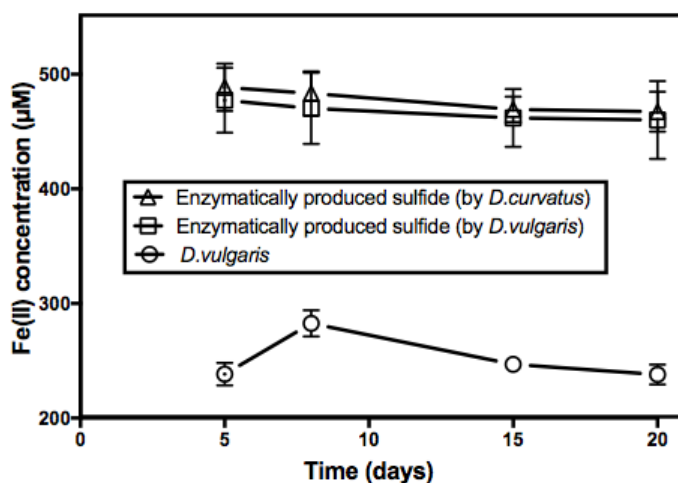


Figure 20. Fe(II) concentrations in all phases over time in different experimental sets (Δ is set 6, \square is set 7, \circ is set 4).

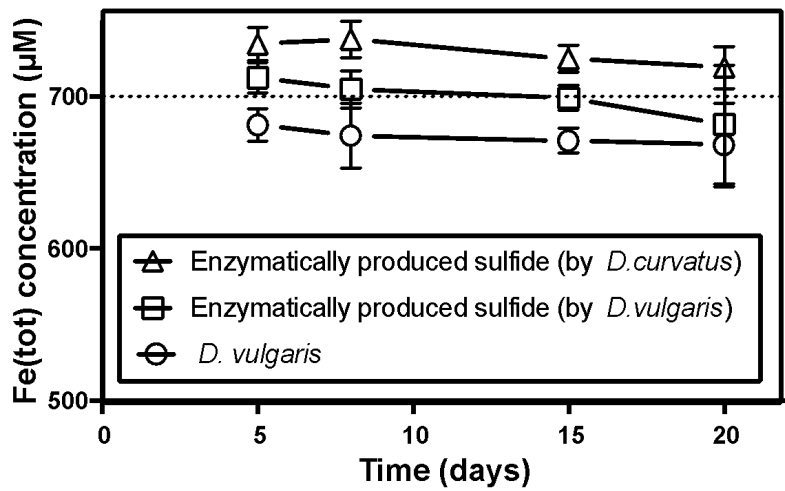


Figure 21. Fe(tot) concentrations in all phases over time in different experimental sets (Δ is set 6, \square is set 7, \circ is set 4).

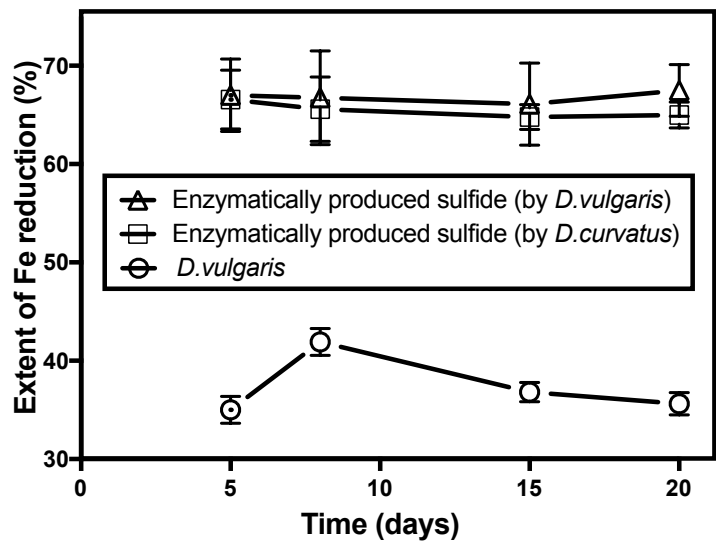


Figure 22. Changes in the extent of Fe(III) reduction over time in different experimental sets (Δ is set 7, \square is set 6 and \circ is set 4).

The ratio of ferrous iron [Fe(II)] to total iron [Fe(tot)] was greater in the aqueous phase than in the solid phase, and sorbed Fe existed almost completely as Fe(II). Significant temporal fluctuation in this ratio for the aqueous, sorbed, and solid phases was not observed in experimental sets with enzymatically produced sulphide (Figure 24). However, in the set with *D. vulgaris* (direct enzymatic reduction of Fe), the ratio between Fe(II) and Fe(tot) in all three

phases increased in the first 8 days and then remained at around 100% in the sorbed phase, whereas fluctuations in this ratio occurred in the aqueous and solid phases (Figure 24).

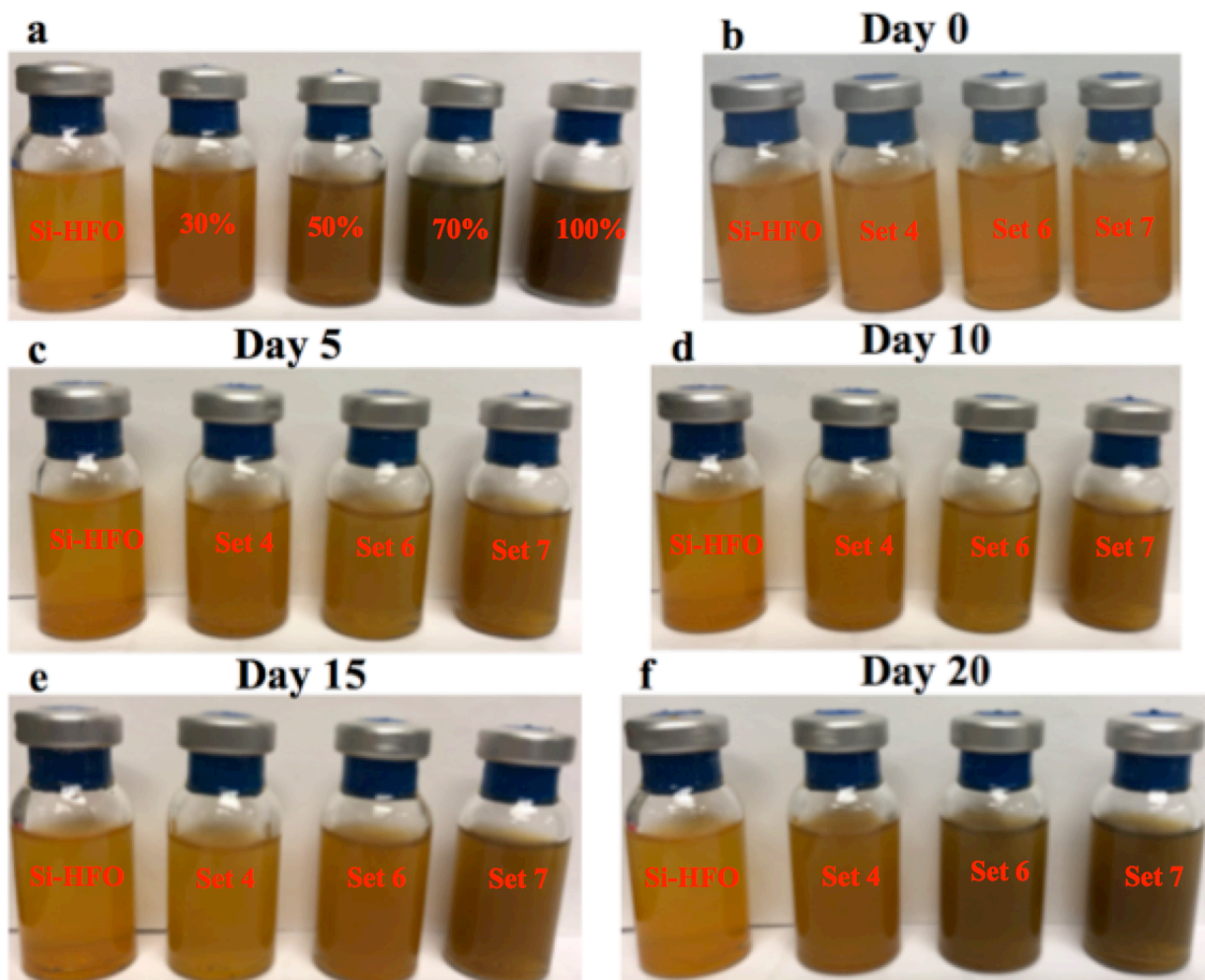


Figure 23. Sample pictures of different experimental sets over time. Panel a shows different extents of Fe(III) reduction. From the left to the right, color of the mixture changes from brownish to dark greenish indicating an increasing extent of Fe(III) reduction. Panels b to f shows changes against time. Pure Si-HFO, set 4, 6 and 7 are shown from left to right in panels b to f.

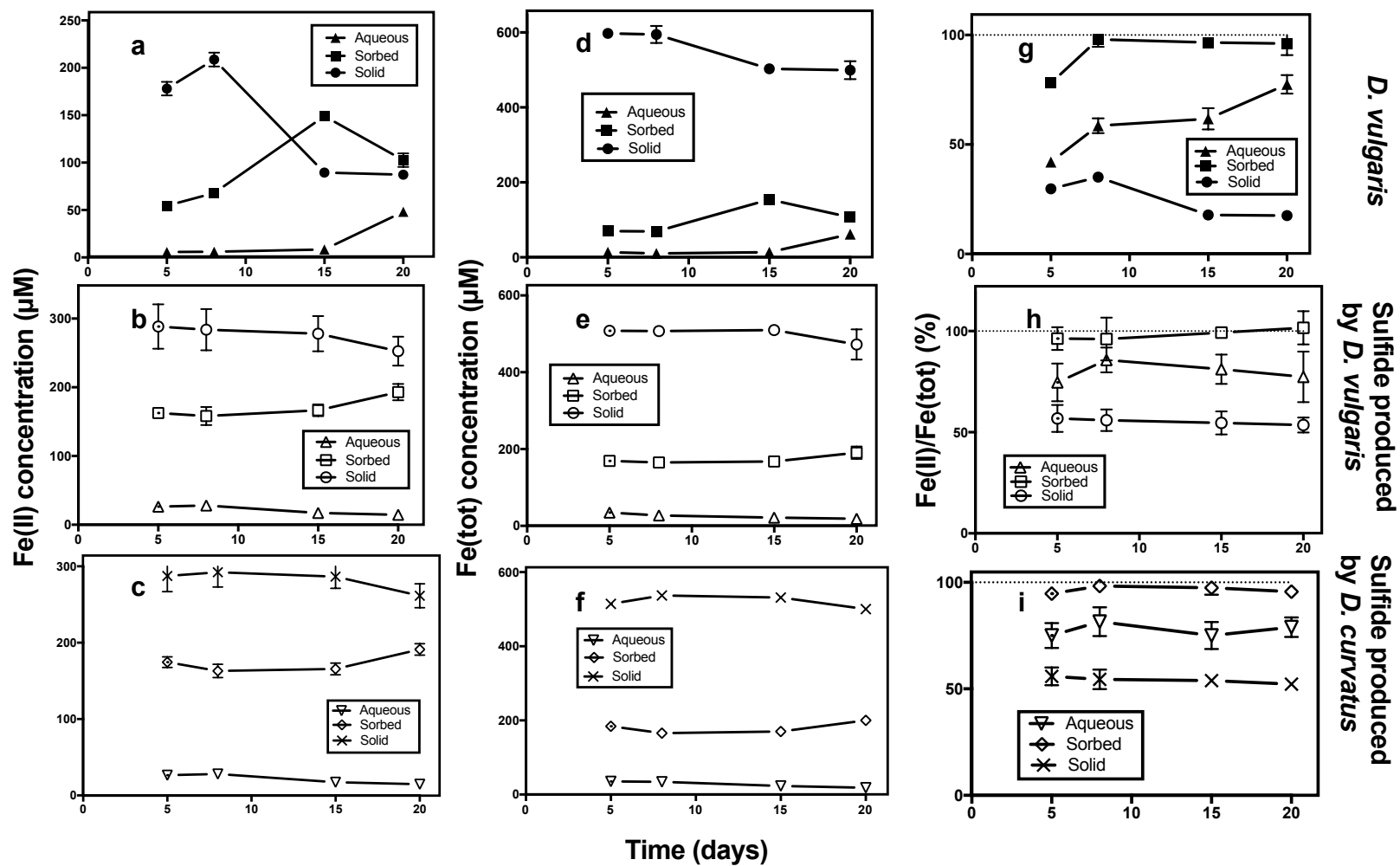


Figure 24. Changes in Fe speciation in aqueous, sorbed, and solid phases over time. Panels a, d and g show the results of set 4. Panels b, e and h show the results of set 7. Panels c, f and i show the results of set 6. Panels a, b, and c show changes of Fe(II) concentration in each phase over time. Panels d, e, and f show changes in the concentration of Fe(tot) in each phase over time. Panels g, h, and i show changes of the % of Fe(tot) that is Fe(II) in each phase over time.

4.3 Fe isotope compositions

Experimental sets 4 and 7 were used to determine the Fe isotope fractionation during Fe(III) reduction caused directly by SRB (*D. vulgaris*) or by enzymatically produced sulfide from SRB, respectively (Figure 23). A similar test using *D. curvatus* cannot be performed because this SRB strain lacks the ability to directly reduce Fe(III) enzymatically. The experimental sets utilized a similar concentration of sulfide (0.2 mM) and Si-HFO (about 0.7 mM), the same temperature (30°C), and the same pH values to probe possible control of Fe and S speciation on the Fe isotope fractionations. The different Fe pools (aqueous, sorbed, and solid) measured in the two experimental sets exhibited distinct isotopic compositions.

The most positive $\delta^{56}\text{Fe}$ values (0.29‰ to 0.95‰; average = $0.48 \pm 0.48\%$, 2σ , $n = 6$) were observed in the solid phase of the set with enzymatically produced sulfide (set 7) (Table 9 and SI Table S11). The most negative $\delta^{56}\text{Fe}$ values (-2.14‰ to -0.30‰; average = $-1.39 \pm 1.30\%$, 2σ , $n = 6$) were observed in the aqueous phase in set 7. The $\delta^{56}\text{Fe}$ values of the sorbed phase of set 7 ranged from -1.28‰ to -0.18‰, with an average of $-0.61 \pm 0.96\%$ (2σ , $n = 4$).

For the set where Fe(III) reduction was carried out directly by *D. vulgaris* (set 4), the $\delta^{56}\text{Fe}$ values of the aqueous phase ranged from -1.63‰ to 0.09‰ (average = $-0.85 \pm 1.50\%$, 2σ , $n = 6$), whereas the $\delta^{56}\text{Fe}$ values of the solid phase ranged from 0.18‰ to 0.51‰ (average = $0.31 \pm 0.20\%$, 2σ , $n = 6$) (Table 9 and SI Table S11). The $\delta^{56}\text{Fe}$ values of the sorbed phase ranged from 0.09‰ to 0.41‰, with an average of $0.23 \pm 0.26\%$ (2σ , $n = 4$).

In summary, the greatest range of $\delta^{56}\text{Fe}$ values was observed in the aqueous phase of the set with enzymatically produced sulfide (set 7). The observed range of aqueous $\delta^{56}\text{Fe}$ values from this set (-2.14‰ to -0.30‰) fall within the range of aqueous Fe isotope compositions in natural freshwater systems (-3.4‰ to 0.8‰) determined by previous studies (Dekov et al., 2014; Guo et al., 2013; Teutsch et al., 2005; Xie et al., 2013; Xie et al., 2014).

Table 9. Fe isotope compositions of different Fe pools.

$\delta^{56}\text{Fe}$ (‰)	<i>D. vulgaris</i> (set 4)			Enzymatically produced sulfide (set 7)		
	Aqueous	Sorbed	Solid	Aqueous	Sorbed	Solid
Min	-1.63	0.09	0.18	-2.14	-1.28	0.29
Max	0.09	0.41	0.51	-0.30	-0.18	0.95
Avg	-0.85	0.23	0.31	-1.39	-0.61	0.48
2SD	1.50	0.27	0.21	1.29	0.95	0.48

Fe isotope fractionation between different phases without specification of Fe(II) and Fe(III) was calculated and plotted as shown in Figure 25 (SI Table S11). The largest Fe isotope fractionation was -2.61‰ and was observed between the aqueous and solid phase in the set with enzymatically produced sulfide (set 7). The fluctuations of Fe(II) to Fe(tot) ratios in aqueous and solid phases results in variable fractionation factors. The smallest Fe isotope fractionations were observed between the sorbed phase and solid phase in the *D. vulgaris* set (set 4).

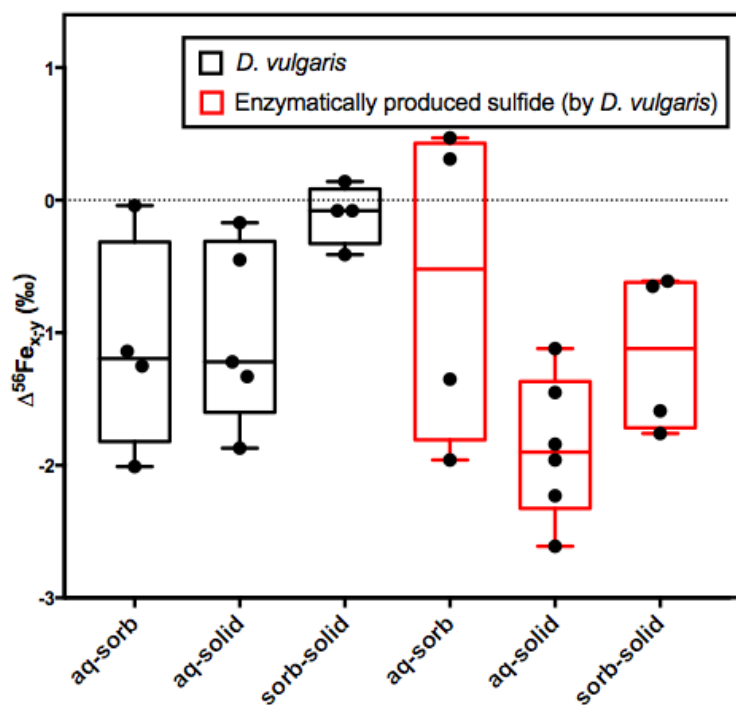


Figure 25. Fe isotope fractionation among different Fe pools (□ shows the results of set 4. □ shows the results of set 7).

The Fe isotopic compositions are not strongly related with time, but instead are correlated with the extent of Fe(III) reduction (Figure 25, 26 and SI Table S11). In general, as the extent of

Fe(III) reduction increased, $\delta^{56}\text{Fe}(\text{tot})_{\text{aq}}$ significantly increased, $\delta^{56}\text{Fe}(\text{tot})_{\text{solid}}$ slightly increased, and $\delta^{56}\text{Fe}(\text{tot})_{\text{sorb}}$ slightly decreased. The Fe isotope compositions in the sorbed and solid phases of set 4 are similar. In set 7, Fe isotope compositions in the sorbed phase partially overlap with the compositions observed in the aqueous phase. Otherwise, Fe in the aqueous phase has significantly lower isotope compositions than that of the sorbed or solid phases in both sets with or without SRB (*D. vulgaris*). The $\delta^{56}\text{Fe}$ in the sorbed phase is higher (all positive values) with cells than without cells (all negative values). These distinct isotopic compositions suggest that Fe isotopes may be used as a tool to trace different pathways of Fe(III) reduction, specifically by enzymatically produced sulfide (without cells) or directly by SRB (with cells).

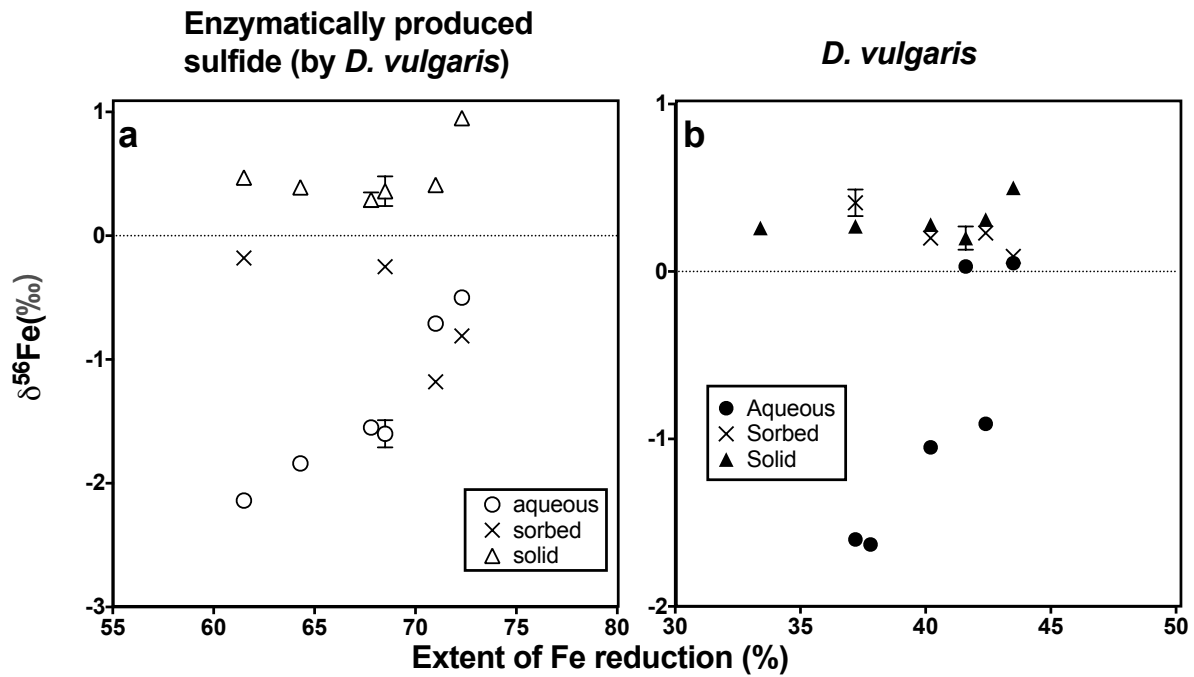


Figure 26. $\delta^{56}\text{Fe}$ among different Fe phases versus the extent of Fe reduction in a) set 7 and b) set 4.

The aqueous and solid phases of all experimental sets consisted of mixtures of both Fe(II) and Fe(III) (Figure 24). To separate Fe(tot) isotope compositions measured on the aqueous and solid phases into the contributions from Fe(II) and Fe(III), three assumptions were made. First, Fe isotope compositions for sorbed Fe(II) are equal to those of sorbed Fe(tot) [$\delta^{56}\text{Fe}_{\text{Fe(II)sorb}} = \delta^{56}\text{Fe}_{\text{Fe(tot)sorb}}$] since it has been observed that sorbed Fe exists almost completely as Fe(II) (Figure 24). Second, Fe isotope fractionation between aqueous Fe(II) and sorbed Fe(II) is -0.20‰ in the

presence of Si and at a pH of 7 [$\Delta^{56}\text{Fe}_{\text{Fe(II)aq}} - \text{Fe}_{\text{Fe(II)sorb}} = -0.20\text{‰}$] (Liu et al., 2015; Wu et al., 2009). Third, Fe(II) in the sorbed phase has the same isotope composition as Fe(II) in the solid phase [$\delta^{56}\text{Fe}_{\text{Fe(II)sorb}} = \delta^{56}\text{Fe}_{\text{Fe(II)solid}}$] (Shi et al., 2016).

With these three assumptions, the Fe isotope compositions of aqueous, sorbed and solid phases were estimated using the Fe(II)/Fe(III) ratios measured in each phase over time. The isotope composition for solid Fe(III) in 0.5 M HCl extracts can be calculated by the following mass balance equation:

$$\delta^{56}\text{Fe}_{\text{solid}} = M_{\text{Fe(II)solid}}/M_{\text{Fe(tot)solid}} \times \delta^{56}\text{Fe}_{\text{sorb}} + M_{\text{Fe(III)solid}}/M_{\text{Fe(tot)solid}} \times \delta^{56}\text{Fe}_{\text{Fe(III)solid}} \quad (7)$$

where $\delta^{56}\text{Fe}_{\text{solid}}$ is the measured Fe(tot) isotope composition of the solid phase, and $M_{\text{Fe(II)solid}}$, $M_{\text{Fe(III)solid}}$ and $M_{\text{Fe(tot)solid}}$ are moles of Fe(II), Fe(III) and Fe(tot) in the solid phase, respectively. The $\delta^{56}\text{Fe}_{\text{sorb}}$ is the measured Fe(tot) isotope composition of the sorbed phase, which is assumed to have a similar isotope composition for the sorbed Fe(II) [$\delta^{56}\text{Fe}_{\text{Fe(II)sorb}}$] and is further equal to the isotope composition for solid Fe(II) [$\delta^{56}\text{Fe}_{\text{Fe(II)solid}}$]. The $\delta^{56}\text{Fe}_{\text{Fe(III)solid}}$ is the isotope composition for solid Fe(III), and is:

$$\delta^{56}\text{Fe}_{\text{Fe(III)solid}} = [\delta^{56}\text{Fe}_{\text{solid}} - M_{\text{Fe(II)solid}}/M_{\text{Fe(tot)solid}} \times \delta^{56}\text{Fe}_{\text{sorb}}]/(M_{\text{Fe(III)solid}}/M_{\text{Fe(tot)solid}}) \quad (8)$$

With the assumption that $\Delta^{56}\text{Fe}_{\text{Fe(II)aq}} - \text{Fe}_{\text{Fe(II)sorb}} = -0.20\text{‰}$, the isotope composition for aqueous Fe(II) can be calculated as follows:

$$\delta^{56}\text{Fe}_{\text{Fe(II)aq}} = \delta^{56}\text{Fe}_{\text{sorb}} - 0.20\text{‰} \quad (9)$$

where $\delta^{56}\text{Fe}_{\text{Fe(II)aq}}$ is the isotope composition of Fe(II) in the aqueous phase.

Once $\delta^{56}\text{Fe}_{\text{Fe(II)aq}}$ was calculated, the isotope composition for aqueous Fe(III) can be calculated using the following mass balance equation:

$$\begin{aligned} \delta^{56}\text{Fe}_{\text{aqueous}} = & M_{\text{Fe(II)aqueous}}/M_{\text{Fe(tot)aqueous}} \times \delta^{56}\text{Fe}_{\text{Fe(II)aq}} \\ & + M_{\text{Fe(III)aqueous}}/M_{\text{Fe(tot)aqueous}} \times \delta^{56}\text{Fe}_{\text{Fe(III)aq}} \end{aligned} \quad (10)$$

where $\delta^{56}\text{Fe}_{\text{aqueous}}$ is the measured Fe(tot) isotope composition of the aqueous phase, $M_{\text{Fe(II)aq}}$, $M_{\text{Fe(III)aq}}$ and $M_{\text{Fe(tot)aq}}$ are moles of Fe(II), Fe(III) and Fe(tot) in the solid phase, respectively. The $\delta^{56}\text{Fe}_{\text{Fe(III)aq}}$ is the isotope composition for aqueous Fe(III), and is:

$$\delta^{56}\text{Fe}_{\text{Fe(III)aq}} = [\delta^{56}\text{Fe}_{\text{aqueous}} - M_{\text{Fe(II)aqueous}}/M_{\text{Fe(tot)aqueous}} \times \delta^{56}\text{Fe}_{\text{Fe(II)aq}}] / (M_{\text{Fe(III)aqueous}}/M_{\text{Fe(tot)aqueous}}) \quad (11)$$

The calculated isotopic compositions of Fe(II) and Fe(III) in each phase were compared. The greatest difference in Fe isotope composition was observed between the aqueous Fe(II) and the solid Fe(III) pools (Figure 27). Fe isotopic fractionation between $\text{Fe(II)}_{\text{aq}}$ and $\text{Fe(III)}_{\text{solid}}$ in the group with enzymatically produced sulfide ranged from -1.22‰ to -4.14‰, with an average of $-2.92 \pm 2.60\text{‰}$ (2σ). Fe isotopic fractionation between $\text{Fe(II)}_{\text{aq}}$ and $\text{Fe(III)}_{\text{solid}}$ in the group with SRB (*D. vulgaris*) was not as large as in the sulfide group, and ranged from -0.04‰ to -0.86‰ with an average of $-0.39 \pm 0.68\text{‰}$ (2σ) (Figure 27). An inverse correlation was observed between $\Delta^{56}\text{Fe}_{\text{Fe(II)aq}-\text{Fe(III)solid}}$ and the extent of Fe(III) reduction (Figure 27). This observation is different from Fe(III) oxyhydroxide mineral reduction by DIRB, where an equilibrium fractionation was observed at around -3‰ and did not change with the extent of Fe(III) reduction (Crosby et al., 2005; Crosby et al., 2007; Percak-Dennett et al., 2011; Wu et al., 2009). In contrast to Fe(III) oxyhydroxide mineral reduction by DIRB, Shi et al. (2016) observed a non-equilibrium Fe isotope fractionation during reduction of structural Fe(III) in layered clay minerals by DIRB. Fe isotope fractionation factors between aqueous Fe(II) and structural Fe(III) increased with an increasing extent of Fe(III) reduction, and ranged from -1.2‰ to +0.8‰.

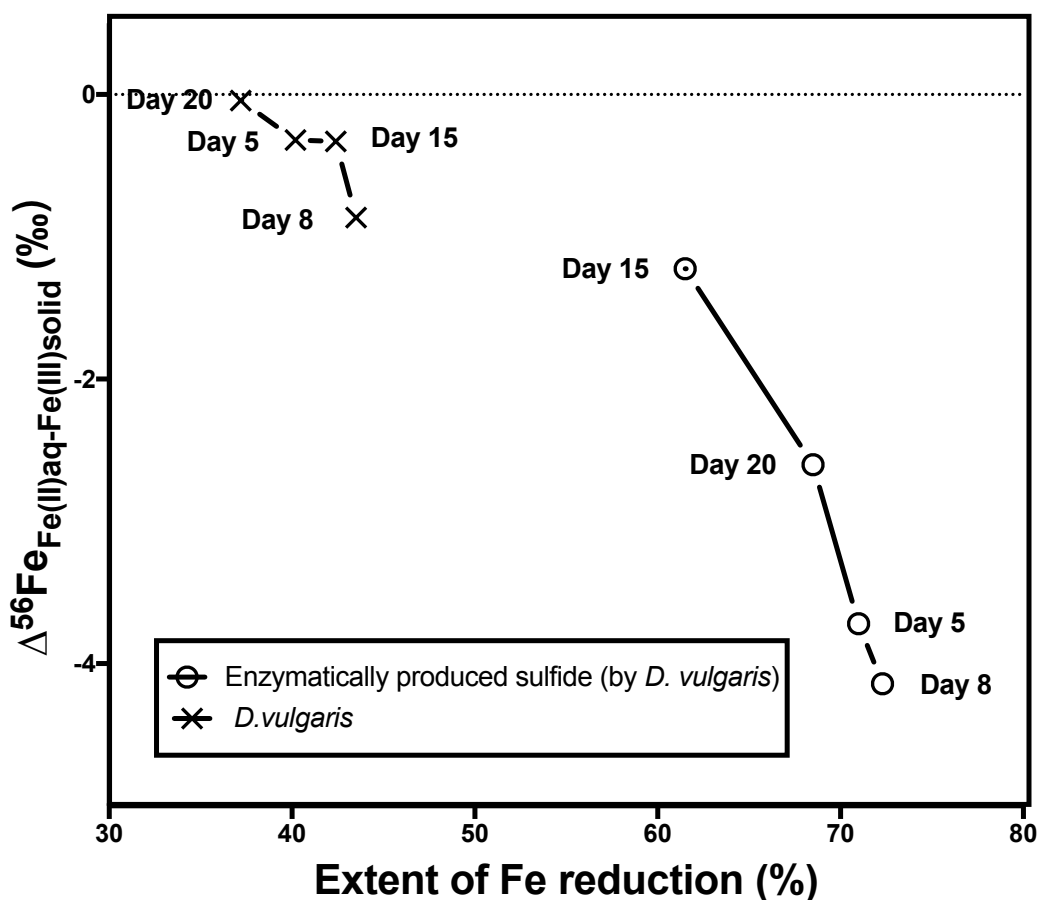


Figure 27. Fe isotopic fractionation between Fe(II)_{aq} and Fe(III)_{solid}. (× is experimental set 7, ○ is experimental set 4).

Earlier studies suggested that $\delta^{56}\text{Fe}$ values are affected by differences in particle coarsening (caused by a combination of particle aggregation and ripening), which can affect isotopic exchange rates (Guilbaud et al., 2010). However, it is not possible to quantify such changes (Wu et al., 2012). The sorption of Fe(II) to Fe(III) minerals was considered as a possible reason for Fe isotope fractionation during microbial Fe reduction by earlier studies (Brantley et al., 2004; Bullen et al., 2001; Icopini et al., 2004). More recent studies concluded that an Fe isotope fractionation ranging from 0.2‰ to 0.9‰ is associated with the sorption of Fe(II) to Fe(III) minerals as well as the electron and atom exchange between the aqueous Fe(II) and solid Fe(III) pools (Crosby et al., 2007; Wu et al., 2009; Wu et al., 2010). This Fe isotope fractionation is much smaller than the fractionation between the aqueous Fe(II) and solid Fe(III) pools caused by most enzymatic or non-enzymatic processes, as measured in this study and previous studies (Crosby et al., 2007; Friedrich et al., 2014; Kai et al., 2015; Reddy et al., 2015; Wu et al., 2011).

Thus, the sorption of Fe(II) to Fe(III) substrates cannot account for the Fe isotope fractionations produced by DIR (Crosby et al., 2005). Equilibrium Fe(II)-HFO fractionation factors of $-2.58 \pm 0.14\text{‰}$ and $-3.17 \pm 0.08\text{‰}$ were obtained for the Si-HFO coprecipitate and HFO plus silica respectively, and indicated a minor isotopic effect by dissolved Si (Wu et al., 2011).

Crosby et al. (2007) pointed out that for experiments using *G. sulfurreducens* and *S. putrefaciens*, the isotopic fractionation between $\text{Fe(II)}_{\text{aq}}$ and $\text{Fe(III)}_{\text{reac}}$ (a reactive ferric Fe component on the Fe oxide surface) was $-2.95 \pm 0.19\text{‰}$ (2σ) and $-2.62 \pm 0.57\text{‰}$ (2σ) with hematite and goethite as the substrate, respectively. Because of these similar values, Crosby et al. (2007) further indicated a similar mechanism of Fe isotope fractionation during DIR of goethite and hematite induced by *G. sulfurreducens* and *S. putrefaciens*. By comparing with the results of abiotic groups, Crosby et al. (2007) determined that the isotopic fractionation between $\text{Fe(II)}_{\text{aq}}$ and $\text{Fe(III)}_{\text{reac}}$ in abiotic systems at room temperature is -3.1‰ and identical within error to the isotopic fractionations measured in biotic groups. Therefore, it was suggested that, independent of bacterial species and ferric Fe substrates, the mechanism that produces Fe isotope fractionation during DIR is the same (Crosby et al., 2007; Dauphas et al., 2017).

Wu et al. (2012) indicated an equilibrium Fe isotope fractionation factor of $-0.32 \pm 0.29\text{‰}$ (2σ) between $\text{Fe}_{\text{aq}}^{2+}$ and mackinawite. This value remained basically unchanged with pH varying from 6 to 8, and temperature varying from 20°C to 35°C . However, this Fe isotope fractionation changed to $-0.64 \pm 0.36\text{‰}$ (2σ) when an equal molarity of free sulphide was added into the system. The decreased $\sim 0.3\text{‰}$ in the magnitude of Fe isotope fractionation was explained by the increases in the proportion of FeS and FeHS^+ in the aqueous phase compared with $\text{Fe(H}_2\text{O)}_6^{2+}$. These Fe species also existed in set 7, thus this model could be a minor factor influencing the Fe isotope fractionation between $\text{Fe(II)}_{\text{aq}}$ and $\text{Fe(III)}_{\text{solid}}$ in set 7.

In this study, the Fe isotope fractionation between $\text{Fe(II)}_{\text{aq}}$ and $\text{Fe(III)}_{\text{solid}}$ in the group with enzymatically produced sulfide and a Si-HFO substrate (set 7) ranged from -1.22‰ to -4.14‰ with an average of $-2.92 \pm 2.60\text{‰}$ (2σ) and is within uncertainty of the Fe isotope fractionations observed by Crosby et al. (2007) in their abiotic and biotic groups. This observation is consistent with the hypothesis of a similar mechanism of Fe isotope fractionation during DIR regardless of the Fe substrate used. An increasing $\Delta^{56}\text{Fe}_{\text{Fe(II)aq}-\text{Fe(III)solid}}$ was observed in this study with the

increasing extent of Fe(III) reduction but not with time (Figure 27). This result indicated a kinetic system instead of an equilibrium system because of the relatively short experimental time period (20 days) applied in this study. Based on previous studies, Fe isotopes should have a redox-based equilibrium fractionation (Dauphas et al., 2017). Thus, if a longer duration (> 100 days) for the experiment was performed, the Fe isotopes may continue to exchange until the system reaches equilibrium; that is, an equilibrium isotope fractionation may ultimately be observed and not change with the extent of Fe(III) reduction (Crosby et al., 2005; Crosby et al., 2007; Percak-Dennett et al., 2011; Wu et al., 2009). Moreover, the Fe isotopic fractionation between Fe(II)_{aq} and Fe(III)_{solid} during direct enzymatic reduction of Fe(III) by SRB (*D. vulgaris*) was $-0.39 \pm 0.68\text{‰}$ (2σ), which is significantly different from the Fe isotope fractionation determined for Fe(III) reduction by enzymatically produced sulfide or DIRB. Hence, Fe isotopes have the potential to be applied as a tracer to determine if Fe(III) reduction was induced by SRB or DIRB at low S concentrations similar to those found in freshwater systems.

5.0 Conclusions

Microbial dissimilatory Fe(III) reduction is a widespread process in anaerobic environments (Thamdrup, 2000), and is associated with SRB (Castro et al., 2000). Previously, based on thermodynamic predictions, it was assumed that microbial respiration of Fe(III) was more prominent than sulfate in all aquatic systems except those with high sulfate concentrations (e.g. marine systems). Hence, in freshwater systems where unusually low sulfate concentrations (< 0.2 mM) occur, it was assumed that sulfide has little influence on Fe cycling (Hansel et al., 2015). Recently, indirect evidence showed that a sulfur-fueled Fe cycle is dominant in not only marine systems but also freshwater systems (Akob et al., 2008; Flynn et al., 2014; Holmkvist et al., 2011; Komlos et al., 2008; Koretsky et al., 2003; Kwon et al., 2014; Osorio et al., 2013; Pester et al., 2012). This result has been explained by the existence of a cryptic sulfur cycle in freshwater systems (Hansel et al., 2015). Furthermore, Hansel et al. (2015) observed that sulfate reduction preceded not only highly crystalline Fe oxide reduction but also ferrihydrite reduction. This inverse redox zonation further argues that, under low-sulfate conditions and independent of the Fe oxide mineralogy, sulfide produced by SRB is a driving factor in Fe(III) reduction. The potential for SRB to enzymatically reduce Fe(III) was studied previously, and although most SRB can enzymatically reduce Fe(III), there are a few strains that cannot (Lovley et al., 1993).

Two strains, *Desulfovibrio vulgaris*, which is capable of reducing Fe(III) minerals enzymatically (Liu et al., 2012), and *Desulfobacter curvatus*, which cannot enzymatically reduce Fe(III) (Lovley et al., 1993), were investigated in this study. Similar extents of Fe(III) reduction were caused by both abiotic and SRB produced sulfide. HFO was shown to be reduced enzymatically by SRB (*D. vulgaris*), but this reaction is less efficient than sulfide induced HFO reduction. The highest extent of Fe(III) reduction was observed in the sets with both SRB (*D. vulgaris* or *D. curvatus*) and 0.2 mM sulfate, indicating the exist of cryptic S cycling under low S conditions.

The Fe isotopic compositions are not strongly related with time, but instead are correlated with the extent of Fe(III) reduction. With increased Fe(III) reduction, $\delta^{56}\text{Fe}_{\text{aq}}$ significantly increased, $\delta^{56}\text{Fe}_{\text{solid}}$ slightly increased, whereas $\delta^{56}\text{Fe}_{\text{orb}}$ slightly decreased. The aqueous phase

has significantly lighter Fe isotope compositions than the sorbed phase and solid phase in both experiments with or without SRB (*D. vulgaris*). The $\delta^{56}\text{Fe}$ in the sorbed phase is higher (all positive values) with cells than without cells (all negative values). The most positive and negative $\delta^{56}\text{Fe}$ values are $0.48 \pm 0.48\text{‰}$ (2σ ; $n=6$) and $-1.39 \pm 1.30\text{‰}$ (2σ ; $n = 6$) in the solid phase and aqueous phase, respectively, from the experiment with SRB produced sulfide. The largest Fe isotope fractionation was -2.61‰ and was observed between the aqueous and solid phase in the set with enzymatically produced sulfide (set 7). The fluctuations of Fe(II) to Fe(tot) ratios in aqueous and solid phases results in variable fractionation factors.

The Fe isotopic fractionation between $\text{Fe(II)}_{\text{aq}}$ and $\text{Fe(III)}_{\text{solid}}$ in the experimental sets where HFO was reduced by enzymatically produced sulfide (by *D. vulgaris*) and directly by SRB (*D. vulgaris*) ranged from -1.22‰ to -4.14‰ with an average of $-2.92 \pm 2.60\text{‰}$ (2σ ; $n=4$), and from -0.04 to -0.86‰ with an average of $-0.39 \pm 0.68\text{‰}$ (2σ ; $n=4$), respectively. Previous studies indicated that $\Delta^{56}\text{Fe}_{\text{Fe(II)}_{\text{aq}}-\text{Fe(III)}_{\text{solid}}}$ was $\sim -3\text{‰}$ for the reduction of either goethite or hematite with the presence of DIRB (e.g. Crosby et al., 2007; Dauphas et al., 2017). Hence, this result confirmed the same mechanism of Fe isotope fractionation during DIR regardless of Fe substrates, but a different mechanism of Fe isotope fractionation occurs during DIR caused by DIRB versus SRB. Thus, Fe isotopes have the potential to be applied as a tracer to evaluate Fe reduction induced 1) enzymatically by SRB versus DIRB; 2) enzymatically by SRB versus non-enzymatically by sulfide. The extent of Fe isotope fractionation during these processes may help shed light on the mechanisms and pathways of electron transfer and atom exchange during sulfur-induced microbial Fe(III) reduction in freshwater systems.

An inverse correlation was observed between $\Delta^{56}\text{Fe}_{\text{Fe(II)}_{\text{aq}}-\text{Fe(III)}_{\text{solid}}}$ and the extent of Fe(III) reduction because of the relatively short time period (20 days) applied in this study. A longer time period could be applied for further experiments to determine whether the Fe isotope fractionation between aqueous phase and solid phase could become stable and $\sim -3\text{‰}$ in the experiments with enzymatically produced sulfide. Transmission electron microscopy (TEM), scanning transmission electron microscopy (STEM), X-ray diffraction (XRD) or scanning electron microscopy (SEM) could be used to analyze the solids, further indicate the structure and the particle size of mineral products, and help determine the Fe reduction mechanisms induced by SRB.

6.0 References

- Akob, D. M., Mills, H. J., Gihring, T. M., Kerkhof, L., Stucki, J. W., Anastácio, A. S., & Kostka, J. E. (2008). Functional diversity and electron donor dependence of microbial populations capable of U (VI) reduction in radionuclide-contaminated subsurface sediments. *Applied and environmental microbiology*, 74(10), 3159-3170.
- Alico, R. K., & Liegey, F. W. (1966). Growth of *Desulfovibrio desulfuricans* under heterotrophic and anaerobic conditions. *Journal of bacteriology*, 91(3), 1112-1114.
- Anbar, A. D., Roe, J. E., Barling, J., & Nealson, K. H. (2000). Nonbiological fractionation of iron isotopes. *Science*, 288(5463), 126-128.
- Baas Becking, L. G. M., & Wood, E. F. (1955). Biological processes in the estuarine environment. I. and II. Ecology of the sulphur cycle.
- Beard, B. L., Johnson, C. M., Cox, L., Sun, H., Nealson, K. H., & Aguilar, C. (1999). Iron isotope biosignatures. *Science*, 285(5435), 1889-1892.
- Beard, B. L., Johnson, C. M., Skulan, J. L., Nealson, K. H., Cox, L., & Sun, H. (2003). Application of Fe isotopes to tracing the geochemical and biological cycling of Fe. *Chemical Geology*, 195(1), 87-117.
- Beard, B. L., & Johnson, C. M. (2004). Fe isotope variations in the modern and ancient earth and other planetary bodies. *Reviews in Mineralogy and Geochemistry*, 55(1), 319-357.
- Bergquist, B. A., & Boyle, E. A. (2006). Iron isotopes in the Amazon River system: weathering and transport signatures. *Earth and Planetary Science Letters*, 248(1), 54-68.
- Bethke, C. M., Sanford, R. A., Kirk, M. F., Jin, Q., & Flynn, T. M. (2011). The thermodynamic ladder in geomicrobiology. *American Journal of Science*, 311(3), 183-210.
- Boland, D. D., Collins, R. N., Glover, C. J., & Waite, T. D. (2013). An in situ quick-EXAFS and redox potential study of the Fe (II)-catalysed transformation of ferrihydrite. *Colloids and Surfaces A: Physicochemical and Engineering Aspects*, 435, 2-8.

- Boland, D. D., Collins, R. N., Miller, C. J., Glover, C. J., & Waite, T. D. (2014). Effect of solution and solid-phase conditions on the Fe (II)-accelerated transformation of ferrihydrite to lepidocrocite and goethite. *Environmental science & technology*, 48(10), 5477-5485.
- Bonneville, S., Behrends, T., Van Cappellen, P., Hyacinthe, C., & Roling, W. F. (2006). Reduction of Fe (III) colloids by *Shewanella putrefaciens*: a kinetic model. *Geochimica et cosmochimica acta*, 70(23), 5842-5854.
- Brantley, S. L., Liermann, L., & Bullen, T. D. (2001). Fractionation of Fe isotopes by soil microbes and organic acids. *Geology*, 29(6), 535-538.
- Bullen, T. D., White, A. F., Childs, C. W., Vivit, D. V., & Schulz, M. S. (2001). Demonstration of significant abiotic iron isotope fractionation in nature. *Geology*, 29(8), 699-702.
- Busigny, V., Planavsky, N. J., Jézéquel, D., Crowe, S., Louvat, P., Moureau, J., & Lyons, T. W. (2014). Iron isotopes in an Archean ocean analogue. *Geochimica et Cosmochimica Acta*, 133, 443-462.
- Canfield, D. E. (2004). The evolution of the Earth surface sulfur reservoir. *American Journal of Science*, 304(10), 839-861.
- Canfield, D. E., Raiswell, R., & Bottrell, S. H. (1992). The reactivity of sedimentary iron minerals toward sulfide. *American Journal of Science*, 292(9), 659-683.
- Castro, H. F., Williams, N. H., & Ogram, A. (2000). Phylogeny of sulfate-reducing bacteria. *FEMS Microbiology Ecology*, 31(1), 1-9.
- Champ, D. R., Gulens, J., & Jackson, R. E. (1979). Oxidation–reduction sequences in ground water flow systems. *Canadian Journal of earth sciences*, 16(1), 12-23.
- Chen, Y., Su, S., He, Y., Li, S., Hou, J., Feng, S., & Gao, K. (2014). Fe isotope compositions and implications on mineralization of Xishimen iron deposit in Wuan, Hebei. *Acta Petrolog Sinica*, 30, 3443-3454.
- Chever, F., Rouxel, O. J., Croot, P. L., Ponzevera, E., Wuttig, K., & Auro, M. (2015). Total dissolvable and dissolved iron isotopes in the water column of the Peru upwelling regime. *Geochimica et Cosmochimica Acta*, 162, 66-82.

- Clesceri, L., Greenberg, A. E., & Trussell, R. R. (1989). Standard methods for water and wastewater examination. *APHA: New York*.
- Clesceri, L. S. (1998). Collection and preservation of samples and Metals. *Standard Methods for the Examination of Water and Wastewater, Edition, 20*, 1-27.
- Cline, J. D. (1969). Spectrophotometric determination of hydrogen sulfide in natural waters. *Limnology and Oceanography*, *14*(3), 454-458.
- Conway, T. M., & John, S. G. (2015). The cycling of iron, zinc and cadmium in the North East Pacific Ocean—Insights from stable isotopes. *Geochimica et Cosmochimica Acta*, *164*, 262-283.
- Craddock, P. R., & Dauphas, N. (2011). Iron isotopic compositions of geological reference materials and chondrites. *Geostandards and Geoanalytical Research*, *35*(1), 101-123.
- Croal, L. R., Johnson, C. M., Beard, B. L., & Newman, D. K. (2004). Iron isotope fractionation by Fe (II)-oxidizing photoautotrophic bacteria. *Geochimica et cosmochimica acta*, *68*(6), 1227-1242.
- Crosby, H. A., Johnson, C. M., Roden, E. E., & Beard, B. L. (2005). Coupled Fe (II)– Fe (III) electron and atom exchange as a mechanism for Fe isotope fractionation during dissimilatory iron oxide reduction. *Environmental science & technology*, *39*(17), 6698-6704.
- Crosby, H. A., Roden, E. E., Johnson, C. M., & Beard, B. L. (2007). The mechanisms of iron isotope fractionation produced during dissimilatory Fe (III) reduction by *Shewanella putrefaciens* and *Geobacter sulfurreducens*. *Geobiology*, *5*(2), 169-189.
- Czaja, A. D., Johnson, C. M., Beard, B. L., Eigenbrode, J. L., Freeman, K. H., & Yamaguchi, K. E. (2010). Iron and carbon isotope evidence for ecosystem and environmental diversity in the ~ 2.7 to 2.5 Ga Hamersley Province, Western Australia. *Earth and Planetary Science Letters*, *292*(1), 170-180.
- Czaja, A. D., Johnson, C. M., Roden, E. E., Beard, B. L., Voegelin, A. R., Nägler, T. F., & Wille, M. (2012). Evidence for free oxygen in the Neoproterozoic ocean based on coupled iron–molybdenum isotope fractionation. *Geochimica et Cosmochimica Acta*, *86*, 118-137.

- Dauphas, N., John, S. G., & Rouxel, O. (2017). Iron isotope systematics. *Reviews in Mineralogy and Geochemistry*, 82(1), 415-510.
- Dekov, V. M., Vanlierde, E., Billström, K., Garbe-Schönberg, C. D., Weiss, D. J., Rotondo, G. G., & Van Grieken, R. (2014). Ferrihydrite precipitation in groundwater-fed river systems (Nete and Demer river basins, Belgium): Insights from a combined Fe-Zn-Sr-Nd-Pb-isotope study. *Chemical Geology*, 386, 1-15.
- Enning, D., & Garrelfs, J. (2014). Corrosion of iron by sulfate-reducing bacteria: new views of an old problem. *Applied and environmental microbiology*, 80(4), 1226-1236.
- Escoube, R., Rouxel, O. J., Sholkovitz, E., & Donard, O. F. (2009). Iron isotope systematics in estuaries: The case of North River, Massachusetts (USA). *Geochimica et Cosmochimica Acta*, 73(14), 4045-4059.
- Fehr, M. A., Andersson, P. S., Halenius, U., & Morth, C. M. (2008). Iron isotope variations in Holocene sediments of the Gotland Deep, Baltic Sea. *Geochimica et Cosmochimica Acta*, 72(3), 807-826.
- Fehr, M. A., Andersson, P. S., Halenius, U., Gustafsson, O., & Morth, C. M. (2010). Iron enrichments and Fe isotopic compositions of surface sediments from the Gotland Deep, Baltic Sea. *Chemical Geology*, 277(3), 310-322.
- Fischer, E. (1883). Bildung von methylenblau als reaktion auf schwefelwasserstoff. *European Journal of Inorganic Chemistry*, 16(2), 2234-2236.
- Flynn, T. M., O'Loughlin, E. J., Mishra, B., DiChristina, T. J., & Kemner, K. M. (2014). Sulfur-mediated electron shuttling during bacterial iron reduction. *Science*, 344(6187), 1039-1042.
- Froelich, P., Klinkhammer, G. P., Bender, M. L., Luedtke, N. A., Heath, G. R., Cullen, D., & Maynard, V. (1979). Early oxidation of organic matter in pelagic sediments of the eastern equatorial Atlantic: suboxic diagenesis. *Geochimica et cosmochimica acta*, 43(7), 1075-1090.
- Gelting, J., Breitbarth, E., Stolpe, B., Hassellöv, M., & Ingri, J. (2010). Fractionation of iron species and iron isotopes in the Baltic Sea euphotic zone. *Biogeosciences*, 7(8), 2489.

- Guelke, M., & Von Blanckenburg, F. (2007). Fractionation of stable iron isotopes in higher plants. *Environmental science & technology*, 41(6), 1896-1901.
- Guilbaud, R., Butler, I. B., Ellam, R. M., & Rickard, D. (2010). Fe isotope exchange between Fe (II) aq and nanoparticulate mackinawite (FeS m) during nanoparticle growth. *Earth and Planetary Science Letters*, 300(1), 174-183.
- Guo, H., Liu, C., Lu, H., Wanty, R. B., Wang, J., & Zhou, Y. (2013). Pathways of coupled arsenic and iron cycling in high arsenic groundwater of the Hetao basin, Inner Mongolia, China: An iron isotope approach. *Geochimica et Cosmochimica Acta*, 112, 130-145.
- Hansel, C. M., Benner, S. G., & Fendorf, S. (2005). Competing Fe (II)-induced mineralization pathways of ferrihydrite. *Environmental Science & Technology*, 39(18), 7147-7153.
- Hansel, C. M., Lentini, C. J., Tang, Y., Johnston, D. T., Wankel, S. D., & Jardine, P. M. (2015). Dominance of sulfur-fueled iron oxide reduction in low-sulfate freshwater sediments. *The ISME journal*, 9(11), 2400-2412.
- Heimann, A., Johnson, C. M., Beard, B. L., Valley, J. W., Roden, E. E., Spicuzza, M. J., & Beukes, N. J. (2010). Fe, C, and O isotope compositions of banded iron formation carbonates demonstrate a major role for dissimilatory iron reduction in ~ 2.5 Ga marine environments. *Earth and Planetary Science Letters*, 294(1), 8-18.
- Hobbie, J. E., Daley, R. J., & Jasper, S. (1977). Use of nuclepore filters for counting bacteria by fluorescence microscopy. *Applied and environmental microbiology*, 33(5), 1225-1228.
- Hoehler, T. M., Alperin, M. J., Albert, D. B., & Martens, C. S. (1998). Thermodynamic control on hydrogen concentrations in anoxic sediments. *Geochimica et cosmochimica acta*, 62(10), 1745-1756.
- Holmkvist, L., Ferdelman, T. G., & Jorgensen, B. B. (2011). A cryptic sulfur cycle driven by iron in the methane zone of marine sediment (Aarhus Bay, Denmark). *Geochimica et Cosmochimica Acta*, 75(12), 3581-3599.
- Homoky, W. B., Severmann, S., Mills, R. A., Statham, P. J., & Fones, G. R. (2009). Pore-fluid Fe isotopes reflect the extent of benthic Fe redox recycling: Evidence from continental shelf and deep-sea sediments. *Geology*, 37(8), 751-754.

- Homoky, W. B., John, S. G., Conway, T. M., & Mills, R. A. (2013). Distinct iron isotopic signatures and supply from marine sediment dissolution. *Nature communications*, 4.
- Huang, F., Zhang, Z., Lundstrom, C. C., & Zhi, X. (2011). Iron and magnesium isotopic compositions of peridotite xenoliths from Eastern China. *Geochimica et Cosmochimica Acta*, 75(12), 3318-3334.
- Ingri, J., Malinovsky, D., Rodushkin, I., Baxter, D. C., Widerlund, A., Andersson, P., ... & Öhlander, B. (2006). Iron isotope fractionation in river colloidal matter. *Earth and Planetary Science Letters*, 245(3), 792-798.
- Jakobsen, R., & Postma, D. (1999). Redox zoning, rates of sulfate reduction and interactions with Fe-reduction and methanogenesis in a shallow sandy aquifer, Romo, Denmark. *Geochimica et Cosmochimica Acta*, 63(1), 137-151.
- Jenkyns, H. C., Matthews, A., Tsikos, H., & Erel, Y. (2007). Nitrate reduction, sulfate reduction, and sedimentary iron isotope evolution during the Cenomanian-Turonian oceanic anoxic event. *Paleoceanography*, 22(3).
- John, S. G. (2012). Optimizing sample and spike concentrations for isotopic analysis by double-spike ICPMS. *Journal of Analytical Atomic Spectrometry*, 27(12), 2123-2131.
- John, S. G., & Adkins, J. (2012). The vertical distribution of iron stable isotopes in the North Atlantic near Bermuda. *Global Biogeochemical Cycles*, 26(2).
- Johnson, C. M., Skulan, J. L., Beard, B. L., Sun, H., Nealson, K. H., & Braterman, P. S. (2002). Isotopic fractionation between Fe (III) and Fe (II) in aqueous solutions. *Earth and Planetary Science Letters*, 195(1), 141-153.
- Johnson, C. M., Beard, B. L., Roden, E. E., Newman, D. K., & Nealson, K. H. (2004). Isotopic constraints on biogeochemical cycling of Fe. *Reviews in mineralogy and geochemistry*, 55(1), 359-408.
- Johnson, C. M., Roden, E. E., Welch, S. A., & Beard, B. L. (2005). Experimental constraints on Fe isotope fractionation during magnetite and Fe carbonate formation coupled to dissimilatory hydrous ferric oxide reduction. *Geochimica et Cosmochimica Acta*, 69(4), 963-993.

- Johnson, C. M., Beard, B. L., & Roden, E. E. (2008). The iron isotope fingerprints of redox and biogeochemical cycling in modern and ancient Earth. *Annu. Rev. Earth Planet. Science*, *36*, 457-493.
- Johnson, C. M., Ludois, J. M., Beard, B. L., Beukes, N. J., & Heimann, A. (2013). Iron formation carbonates: Paleoceanographic proxy or recorder of microbial diagenesis?. *Geology*, *41*(11), 1147-1150.
- Jambor, J. L., & Dutrizac, J. E. (1998). Occurrence and constitution of natural and synthetic ferrihydrite, a widespread iron oxyhydroxide. *Chemical Reviews*, *98*(7), 2549-2586.
- Kendall, C., & McDonnell, J. J. (Eds.). (2012). *Isotope tracers in catchment hydrology*. Elsevier.
- Komlos, J., Moon, H. S., & Jaffe, P. R. (2008). Effect of sulfate on the simultaneous bioreduction of iron and uranium. *Journal of environmental quality*, *37*(6), 2058-2062.
- Koretsky, C. M., Moore, C. M., Lowe, K. L., Meile, C., DiChristina, T. J., & Van Cappellen, P. (2003). Seasonal oscillation of microbial iron and sulfate reduction in saltmarsh sediments (Sapelo Island, GA, USA). *Biogeochemistry*, *64*(2), 179-203.
- Kwon, M. J., Boyanov, M. I., Antonopoulos, D. A., Brulc, J. M., Johnston, E. R., Skinner, K. A., & O'Loughlin, E. J. (2014). Effects of dissimilatory sulfate reduction on Fe III (hydr) oxide reduction and microbial community development. *Geochimica et Cosmochimica Acta*, *129*, 177-190.
- Labatut, M., Lacan, F., Pradoux, C., Chmeleff, J., Radic, A., Murray, J. W., & Thil, F. (2014). Iron sources and dissolved-particulate interactions in the seawater of the Western Equatorial Pacific, iron isotope perspectives. *Global Biogeochemical Cycles*, *28*(10), 1044-1065.
- Lalonde, K., Mucci, A., Ouellet, A., & Gelinas, Y. (2012). Preservation of organic matter in sediments promoted by iron. *Nature*, *483*(7388), 198-200.
- Li, W., Beard, B. L., & Johnson, C. M. (2015). Biologically recycled continental iron is a major component in banded iron formations. *Proceedings of the National Academy of Sciences*, *112*(27), 8193-8198.

- Liu, D., Dong, H., Bishop, M. E., Zhang, J., Wang, H., Xie, S., & Eberl, D. D. (2012). Microbial reduction of structural iron in interstratified illite-smectite minerals by a sulfate-reducing bacterium. *Geobiology*, *10*(2), 150-162.
- Liu, K., Wu, L., Couture, R. M., Li, W., & Van Cappellen, P. (2015). Iron isotope fractionation in sediments of an oligotrophic freshwater lake. *Earth and Planetary Science Letters*, *423*, 164-172.
- Lovley, D. R., & Phillips, E. J. (1987). Competitive mechanisms for inhibition of sulfate reduction and methane production in the zone of ferric iron reduction in sediments. *Applied and Environmental Microbiology*, *53*(11), 2636-2641.
- Lovley, D. R., Roden, E. E., Phillips, E. J. P., & Woodward, J. C. (1993). Enzymatic iron and uranium reduction by sulfate-reducing bacteria. *Marine Geology*, *113*(1-2), 41-53.
- Malinovsky, D. N., Rodyushkin, I. V., Shcherbakova, E. P., Ponter, C., Ohlander, B., & Ingri, J. (2005). Fractionation of Fe isotopes as a result of redox processes in a basin. *Geochemistry International*, *43*(8), 797-803.
- Mansfeldt, T., Schuth, S., Häusler, W., Wagner, F. E., Kaufhold, S., & Overesch, M. (2012). Iron oxide mineralogy and stable iron isotope composition in a Gleysol with petrogleyic properties. *Journal of soils and sediments*, *12*(1), 97-114.
- Marin-Carbonne, J., Rollion-Bard, C., Bekker, A., Rouxel, O., Agangi, A., Cavalazzi, B., & McKeegan, K. D. (2014). Coupled Fe and S isotope variations in pyrite nodules from Archean shale. *Earth and Planetary Science Letters*, *392*, 67-79.
- Mikucki, J. A., Pearson, A., Johnston, D. T., Turchyn, A. V., Farquhar, J., Schrag, D. P., & Lee, P. A. (2009). A Contemporary Microbially Maintained Subglacial Ferrous" Ocean". *Science*, *324*(5925), 397-400.
- Moeller, K., Schoenberg, R., Grenne, T., Thorseth, I. H., Drost, K., & Pedersen, R. B. (2014). Comparison of iron isotope variations in modern and Ordovician siliceous Fe oxyhydroxide deposits. *Geochimica et cosmochimica acta*, *126*, 422-440.
- Nealson, K. H., & Myers, C. R. (1990). Iron reduction by bacteria: a potential role in the genesis of banded iron formations. *American Journal of Science*, *290*, 35-45.

- Nishizawa, M., Yamamoto, H., Ueno, Y., Tsuruoka, S., Shibuya, T., Sawaki, Y., & Maruyama, S. (2010). Grain-scale iron isotopic distribution of pyrite from Precambrian shallow marine carbonate revealed by a femtosecond laser ablation multicollector ICP-MS technique: possible proxy for the redox state of ancient seawater. *Geochimica et Cosmochimica Acta*, 74(9), 2760-2778.
- Osorio, H., Mangold, S., Denis, Y., Ñancucheo, I., Esparza, M., Johnson, D. B., & Holmes, D. S. (2013). Anaerobic sulfur metabolism coupled to dissimilatory iron reduction in the extremophile *Acidithiobacillus ferrooxidans*. *Applied and environmental microbiology*, 79(7), 2172-2181.
- Patrick, W. H., & Henderson, R. E. (1981). Reduction and reoxidation cycles of manganese and iron in flooded soil and in water solution. *Soil Science Society of America Journal*, 45(5), 855-859.
- Percak-Dennett, E. M., Beard, B. L., Xu, H., Konishi, H., Johnson, C. M., & Roden, E. E. (2011). Iron isotope fractionation during microbial dissimilatory iron oxide reduction in simulated Archaean seawater. *Geobiology*, 9(3), 205-220.
- Percak-Dennett, E. M., Loizeau, J. L., Beard, B. L., Johnson, C. M., & Roden, E. E. (2013). Iron isotope geochemistry of biogenic magnetite-bearing sediments from the Bay of Vidy, Lake Geneva. *Chemical Geology*, 360, 32-40.
- Pester, M., Knorr, K. H., Friedrich, M. W., Wagner, M., & Loy, A. (2012). Sulfate-reducing microorganisms in wetlands—fameless actors in carbon cycling and climate change. *Frontiers in Microbiology*, 3.
- Planavsky, N., Rouxel, O. J., Bekker, A., Hofmann, A., Little, C. T., & Lyons, T. W. (2012). Iron isotope composition of some Archean and Proterozoic iron formations. *Geochimica et Cosmochimica Acta*, 80, 158-169.
- Poitrasson, F., Delpech, G., & Gregoire, M. (2013). On the iron isotope heterogeneity of lithospheric mantle xenoliths: implications for mantle metasomatism, the origin of basalts and the iron isotope composition of the Earth. *Contributions to Mineralogy and Petrology*, 165(6), 1243-1258.

- Postma, D., & Jakobsen, R. (1996). Redox zonation: equilibrium constraints on the Fe (III)/SO₄-reduction interface. *Geochimica et Cosmochimica Acta*, 60(17), 3169-3175.
- Radic, A., Lacan, F., & Murray, J. W. (2011). Iron isotopes in the seawater of the equatorial Pacific Ocean: new constraints for the oceanic iron cycle. *Earth and Planetary Science Letters*, 306(1), 1-10.
- Raye, U., Pufahl, P. K., Kyser, T. K., Ricard, E., & Hiatt, E. E. (2015). The role of sedimentology, oceanography, and alteration on the $\delta^{56}\text{Fe}$ value of the Sokoman iron formation, Labrador trough, Canada. *Geochimica et Cosmochimica Acta*, 164, 205-220.
- Roe, J. E., Anbar, A. D., & Barling, J. (2003). Nonbiological fractionation of Fe isotopes: evidence of an equilibrium isotope effect. *Chemical Geology*, 195(1), 69-85.
- Rouxel, O. J., Bekker, A., & Edwards, K. J. (2005). Iron isotope constraints on the Archean and Paleoproterozoic ocean redox state. *Science*, 307(5712), 1088-1091.
- Rouxel, O., Sholkovitz, E., Charette, M., & Edwards, K. J. (2008). Iron isotope fractionation in subterranean estuaries. *Geochimica et Cosmochimica Acta*, 72(14), 3413-3430.
- Rouxel, O. J., & Auro, M. (2010). Iron Isotope Variations in Coastal Seawater Determined by Multicollector ICP-MS. *Geostandards and Geoanalytical Research*, 34(2), 135-144.
- Scholz, F., Severmann, S., McManus, J., & Hensen, C. (2014). Beyond the Black Sea paradigm: the sedimentary fingerprint of an open-marine iron shuttle. *Geochimica et Cosmochimica Acta*, 127, 368-380.
- Seo, E. Y., Ahn, T. S., & Zo, Y. G. (2010). Agreement, precision, and accuracy of epifluorescence microscopy methods for enumeration of total bacterial numbers. *Applied and environmental microbiology*, 76(6), 1981-199.
- Severmann, S., Johnson, C. M., Beard, B. L., & McManus, J. (2006). The effect of early diagenesis on the Fe isotope compositions of porewaters and authigenic minerals in continental margin sediments. *Geochimica et Cosmochimica Acta*, 70(8).
- Severmann, S., Lyons, T. W., Anbar, A., McManus, J., & Gordon, G. (2008). Modern iron isotope perspective on the benthic iron shuttle and the redox evolution of ancient oceans. *Geology*, 36(6), 487-490.

- Severmann, S., McManus, J., Berelson, W. M., & Hammond, D. E. (2010). The continental shelf benthic iron flux and its isotope composition. *Geochimica et Cosmochimica Acta*, 74(14), 3984-4004.
- Shi, B., Liu, K., Wu, L., Li, W., Smeaton, C. M., Beard, B. L., & Van Cappellen, P. (2016). Iron Isotope Fractionations Reveal a Finite Bioavailable Fe Pool for Structural Fe (III) Reduction in Nontronite. *Environmental science & technology*, 50(16), 8661-8669.
- Skulan, J. L., Beard, B. L., & Johnson, C. M. (2002). Kinetic and equilibrium Fe isotope fractionation between aqueous Fe (III) and hematite. *Geochimica et Cosmochimica Acta*, 66(17), 2995-3015.
- Song, L., Liu, C. Q., Wang, Z. L., Zhu, X., Teng, Y., Liang, L., ... & Li, J. (2011). Iron isotope fractionation during biogeochemical cycle: Information from suspended particulate matter (SPM) in Aha Lake and its tributaries, Guizhou, China. *Chemical geology*, 280(1), 170-179.
- Staubwasser, M., Von Blanckenburg, F., & Schoenberg, R. (2006). Iron isotopes in the early marine diagenetic iron cycle. *Geology*, 34(8), 629-632.
- Steinboefel, G., von Blanckenburg, F., Horn, I., Konhauser, K. O., Beukes, N. J., & Gutzmer, J. (2010). Deciphering formation processes of banded iron formations from the Transvaal and the Hamersley successions by combined Si and Fe isotope analysis using UV femtosecond laser ablation. *Geochimica et Cosmochimica Acta*, 74(9), 2677-2696.
- Stookey, L. L. (1970). Ferrozine---a new spectrophotometric reagent for iron. *Analytical chemistry*, 42(7), 779-781.
- Tangalos, G. E., Beard, B. L., Johnson, C. M., Alpers, C. N., Shelobolina, E. S., Xu, H., & Roden, E. E. (2010). Microbial production of isotopically light iron (II) in a modern chemically precipitated sediment and implications for isotopic variations in ancient rocks. *Geobiology*, 8(3), 197-208.
- Taylor, S. R., & McLennan, S. M. (1985). The continental crust: its composition and evolution.
- Teng, F. Z., Dauphas, N., Helz, R. T., Gao, S., & Huang, S. (2011). Diffusion-driven magnesium and iron isotope fractionation in Hawaiian olivine. *Earth and Planetary Science Letters*, 308(3), 317-324.

- Teutsch, N., Von Gunten, U., Porcelli, D., Cirpka, O. A., & Halliday, A. N. (2005). Adsorption as a cause for iron isotope fractionation in reduced groundwater. *Geochimica et Cosmochimica Acta*, 69(17), 4175-4185.
- Teutsch, N., Schmid, M., Müller, B., Halliday, A. N., Burgmann, H., & Wehrli, B. (2009). Large iron isotope fractionation at the oxic–anoxic boundary in Lake Nyos. *Earth and Planetary Science Letters*, 285(1), 52-60.
- Thamdrup, B., Fossing, H., & Jørgensen, B. B. (1994). Manganese, iron and sulfur cycling in a coastal marine sediment, Aarhus Bay, Denmark. *Geochimica et Cosmochimica Acta*, 58(23), 5115-5129.
- Thamdrup, B. (2000). Bacterial manganese and iron reduction in aquatic sediments. In *Advances in microbial ecology* (pp. 41-84). Springer US.
- Tsikos, H., Matthews, A., Erel, Y., & Moore, J. M. (2010). Iron isotopes constrain biogeochemical redox cycling of iron and manganese in a Palaeoproterozoic stratified basin. *Earth and Planetary Science Letters*, 298(1), 125-134.
- Viollier, E., Inglett, P. W., Hunter, K., Roychoudhury, A. N., & Van Cappellen, P. (2000). The ferrozine method revisited: Fe (II)/Fe (III) determination in natural waters. *Applied geochemistry*, 15(6), 785-790.
- Wang, X., Zhu, M., Lan, S., Ginder-Vogel, M., Liu, F., & Feng, X. (2015). Formation and secondary mineralization of ferrihydrite in the presence of silicate and Mn (II). *Chemical Geology*, 415, 37-46.
- Welch, S. A., Beard, B. L., Johnson, C. M., & Braterman, P. S. (2003). Kinetic and equilibrium Fe isotope fractionation between aqueous Fe (II) and Fe (III). *Geochimica et Cosmochimica Acta*, 67(22), 4231-4250.
- Whitehouse, M. J., & Fedo, C. M. (2007). Microscale heterogeneity of Fe isotopes in > 3.71 Ga banded iron formation from the Isua Greenstone Belt, southwest Greenland. *Geology*, 35(8), 719-722.
- Widdel, F., Kohring, G. W., & Mayer, F. (1983). Studies on dissimilatory sulfate-reducing bacteria that decompose fatty acids. *Archives of Microbiology*, 134(4), 286-294.

- Widdel, F., & Bak, F. (1992). Gram-negative mesophilic sulfate-reducing bacteria. In *The prokaryotes* (pp. 3352-3378). Springer New York.
- Widdel, F., & Pfennig, N. (1977). A new anaerobic, sporing, acetate-oxidizing, sulfate-reducing bacterium, *Desulfotomaculum* (emend.) *acetoxidans*. *Archives of Microbiology*, *112*(1), 119-122.
- Widdel, F., & Pfennig, N. (1981). Sporulation and further nutritional characteristics of *Desulfotomaculum acetoxidans*. *Archives of Microbiology*, *129*(5), 401-402.
- Wiederhold, J. G., Teutsch, N., Kraemer, S. M., Halliday, A. N., & Kretzschmar, R. (2007). Iron isotope fractionation in oxic soils by mineral weathering and podzolization. *Geochimica et Cosmochimica Acta*, *71*(23), 5821-5833.
- Williams, K. H., Long, P. E., Davis, J. A., Wilkins, M. J., N'Guessan, A. L., Steefel, C. I., & McGuinness, L. (2011). Acetate availability and its influence on sustainable bioremediation of uranium-contaminated groundwater. *Geomicrobiology Journal*, *28*(5-6), 519-539.
- World Health Organization. (2004). *Guidelines for drinking-water quality* (Vol. 1). World Health Organization.
- Wu, L., Beard, B. L., Roden, E. E., & Johnson, C. M. (2009). Influence of pH and dissolved Si on Fe isotope fractionation during dissimilatory microbial reduction of hematite. *Geochimical et Cosmochimica Acta*, *73*(19), 5584-5599.
- Wu, L., Beard, B. L., Roden, E. E., & Johnson, C. M. (2011). Stable iron isotope fractionation between aqueous Fe (II) and hydrous ferric oxide. *Environmental science & technology*, *45*(5), 1847-1852.
- Wu, L., Brucker, R. P., Beard, B. L., Roden, E. E., & Johnson, C. M. (2013). Iron isotope characteristics of hot springs at Chocolate Pots, Yellowstone National Park. *Astrobiology*, *13*(11), 1091-1101.
- Wu, L., Druschel, G., Findlay, A., Beard, B. L., & Johnson, C. M. (2012). Experimental determination of iron isotope fractionations among $\text{Fe}_{\text{aq}}^{2+}$ - FeS_{aq} -Mackinawite at low temperatures: Implications for the rock record. *Geochimica et cosmochimica acta*.

- Xie, X., Johnson, T. M., Wang, Y., Lundstrom, C. C., Ellis, A., Wang, X., & Duan, M. (2013). Mobilization of arsenic in aquifers from the Datong Basin, China: evidence from geochemical and iron isotopic data. *Chemosphere*, *90*(6), 1878-1884.
- Xie, X., Johnson, T. M., Wang, Y., Lundstrom, C. C., Ellis, A., Wang, X., & Li, J. (2014). Pathways of arsenic from sediments to groundwater in the hyporheic zone: Evidence from an iron isotope study. *Journal of Hydrology*, *511*, 509-517.
- Yao, W., & Millero, F. J. (1996). Oxidation of hydrogen sulfide by hydrous Fe (III) oxides in seawater. *Marine Chemistry*, *52*(1), 1-16.

Appendix A - Supplementary Information

Table S1. Sulfide concentrations over time in sets initially having 3.2 mM Si-HFO and 0.2 mM Na₂S.

Time (days)	Set 1 (Abiotic) (μM)	Set 5 (<i>D. vulgaris</i>) (μM)	Set 3 (<i>D. curvatus</i>) (μM)
0	200.00	0	0
5 min	4.00	N/A	N/A
1	0.09	6.00	4.02
3	0.17	0.70	0.12
5	N/A	0.02	0.05
10	0.04	0.07	0
15	N/A	0	0.01
20	0.03	0	0

Table S2. Produced Fe(II) concentrations over time in groups initially having 3.2 mM Si-HFO and 0.2 mM Na₂S.

Time (days)	Set 1 (Abiotic) (μM)	Set 5 (<i>D. vulgaris</i>) (μM)	Set 3 (<i>D. curvatus</i>) (μM)	Set 4 (<i>D. vulgaris</i> without S source) (μM)
0	0	0	0	0
5 min	399.2	N/A	N/A	N/A
1	403.0	680.0	454.0	188.1
3	397.3	838.7	677.0	283.1
5	N/A	900.0	811.9	300.6
10	402.1	903.2	855.7	312.5
15	N/A	898.9	860.0	321.2
20	401.1	901.0	868.0	319.9

Table S3. Extent of Fe(III) reduction measured with either *D. vulgaris* (set 4) without S source or SRB (*D. vulgaris*) produced sulfide (set 7) using different concentrations of Si-HFO.

Time (days)	<i>D. vulgaris</i> (set 4)						SRB (<i>D. vulgaris</i>) produced sulfide (set 7)					
	10 mM (%)		3.2 mM (%)		0.7 mM (%)		10 mM (%)		3.2 mM (%)		0.7 mM (%)	
5	3.0	3.1	9.3	9.4	36.0	36.3	4.5	4.7	15.1	14.8	68.8	71.3
8	3.2	3.0	9.4	9.8	41.6	43.5	4.8	4.8	14.9	15.0	72.3	68.9
15	2.8	3.0	10.2	10.0	37.8	35.7	4.6	4.5	14.7	14.8	71.0	67.8
20	3.1	2.9	9.9	10.0	34.9	35.7	4.5	4.3	14.9	15.1	68.5	68.4

***Note: Two measurements for each concentration for each time point.**

Table S4. Fe(II) concentrations measured for different phases over time in sets with 0.7 mM Si-HFO.

	Time (days)	Aqueous Fe(II) (μM)				Sorbed Fe(II) (μM)				Solid Fe(II) (μM)			
Set 4 (<i>D. vulgaris</i>)	5	5.5	6.1	5.4	5.7	54.0	50.5	57.3	56.6	171.2	172.6	185.0	183.4
	8	4.4	8.2	4.7	6.8	63.1	64.0	72.3	72.1	207.5	200.2	209.2	218.2
	15	10.2	7.0	9.7	6.9	153.4	144.3	151.4	147.0	88.6	89.0	91.6	89.0
	20	46.0	52.1	43.9	50.3	100.2	93.5	107.3	109.2	81.2	91.3	87.3	89.6
Set 7 (Sulfide produced by <i>D. vulgaris</i>)	5	21.8	22.8	31.1	30.0	167.8	153.7	168.1	160.5	263.8	307.1	258.2	324.3
	8	20.8	23.4	31.3	36.3	172.0	167.1	146.8	147.3	255.3	308.5	260.7	311.2
	15	17.8	15.3	18.9	17.1	157.1	164.0	167.3	177.7	270.2	312.2	251.0	278.8
	20	12.2	14.5	14.6	16.2	184.7	181.6	206.9	198.6	236.5	233.1	275.5	265.7
Set 6 (Sulfide produced by <i>D. curvatus</i>)	5	24.6	25.1	28.7	27.9	181.2	179.8	168.1	169.1	278.9	293.2	264.8	312.9
	8	25.8	22.7	32.1	31.4	169.2	167.1	150.2	165.8	266.7	289.2	302.1	311.1
	15	17.8	15.3	18.9	17.1	160.1	159.7	166.6	176.1	280.9	309.2	278.2	277.7
	20	13.1	14.5	14.7	16.3	191.2	181.6	192.4	199.9	241.3	266.6	278.9	259.3

*Note: Four measurements for each phase for each time point.

Table S5. Fe(II) concentrations in all phases in sets with 0.7 mM Si-HFO.

Time (days)	Set 4 (<i>D. vulgaris</i>) (μM)				Set 7 (Sulfide produced by <i>D. vulgaris</i>) (μM)				Set 6 (Sulfide produced by <i>D. curvatus</i>) (μM)			
5	230.7	229.3	247.7	245.8	453.4	483.6	457.4	514.8	484.7	498.1	461.6	509.9
8	275.0	272.3	286.3	297.1	448.1	499.0	438.8	494.8	461.7	479.0	484.4	508.3
15	252.1	240.3	252.6	242.9	445.0	491.5	437.2	473.6	458.8	484.2	463.7	470.9
20	227.4	236.9	238.4	249.0	433.4	429.1	497.0	480.6	445.6	462.6	486.0	475.5

*Note: Four measurements for each set for each time point.

Table S6. Fe(tot) concentrations measured for different phases over time in sets with 0.7 mM Si-HFO.

	Time (days)	Aqueous Fe(tot) (μM)				Sorbed Fe(tot) (μM)				Solid Fe(tot) (μM)			
Set 4 (<i>D. vulgaris</i>)	5	12.6	13.9	13.1	14.6	68.2	67.2	72.5	71.8	610.6	586.8	602.2	590.9
	8	7.9	13.9	7.4	12.2	66.0	67.4	71.1	72.3	609.5	561.3	609.3	598.1
	15	15.4	10.6	16.6	12.1	155.2	150.9	156.8	153.9	501.6	500.2	494.5	515.2
	20	61.0	62.9	60.0	64.0	99.7	105.6	108.1	113.5	494.8	467.6	515.7	519.3
Set 7 (Sulfide produced by <i>D. vulgaris</i>)	5	28.2	41.4	27.2	42.1	172.1	160.6	163.5	180.0	501.6	506.2	518.3	505.7
	8	20.7	33.2	20.6	34.5	171.1	153.5	171.9	164.3	502.7	507.8	503.1	514.8
	15	20.8	18.2	22.3	24.3	157.0	169.7	170.0	174.4	516.3	504.7	518.4	499.4
	20	19.6	19.3	18.3	17.5	172.0	190.7	188.3	211.2	490.3	416.8	508.3	473.7
Set 6 (Sulfide produced by <i>D. curvatus</i>)	5	35.2	35.7	36.8	34.1	188.2	192.1	177.0	180.2	510.0	521.6	516.6	509.2
	8	29.1	31.2	37.9	39.2	171.1	169.3	158.6	164.3	552.3	537.3	527.2	532.1
	15	21.3	22.4	25.3	23.2	161.1	166.9	177.7	174.4	534.2	543.1	528.8	519.9
	20	17.3	19.3	18.3	19.2	193.2	191.7	204.2	211.4	493.1	499.9	508.3	500.2

***Note: Four measurements for each phase for each time point.**

Table S7. Fe(tot) concentrations in all phases in sets with 0.7 mM Si-HFO.

Time (days)	Set 4 (<i>D. vulgaris</i>) (μM)				Set 7 (Sulfide produced by <i>D. vulgaris</i>) (μM)				Set 6 (Sulfide produced by <i>D. curvatus</i>) (μM)			
5	691.4	667.9	687.8	677.3	704.9	702.4	719.0	722.5	733.4	749.4	730.4	723.5
8	683.4	642.6	687.7	682.5	699.6	690.2	710.6	718.0	752.5	737.8	723.7	735.6
15	672.3	661.8	667.9	681.2	694.1	692.6	710.7	698.2	716.6	732.4	731.8	717.5
20	655.5	636.1	683.9	696.8	681.9	626.7	714.9	702.4	703.6	710.9	730.8	730.8

***Note: Four measurements for each phase for each time point.**

Table S8. Fe(II)/Fe(tot) for different phases over time in sets with 0.7 mM Si-HFO.

	Time (days)	Aqueous Fe(II)/Fe(tot) (%)				Sorbed Fe(II)/Fe(tot) (%)				Solid Fe(II)/Fe(tot) (%)			
Set 4 (<i>D. vulgaris</i>)	5	43.6	44.1	41.0	39.3	79.1	75.2	79.0	78.8	28.0	29.4	30.7	31.0
	8	56.1	58.8	63.3	56.0	95.5	94.9	101.8	99.7	34.0	35.7	34.3	36.5
	15	66.1	65.7	58.3	56.8	98.8	95.6	96.6	95.5	17.7	17.8	18.5	17.3
	20	75.4	82.9	73.1	78.5	100.5	88.6	99.2	96.2	16.4	19.5	16.9	17.2
Set 7 (Sulfide produced by <i>D. vulgaris</i>)	5	69.7	64.0	83.5	81.5	97.5	95.7	102.8	89.1	52.6	60.7	49.8	64.1
	8	80.5	81.1	88.0	93.4	100.5	108.8	85.4	89.7	50.8	60.7	51.8	60.4
	15	85.6	84.1	84.7	70.3	100.1	96.7	98.4	101.9	52.3	61.9	48.4	55.8
	20	62.2	75.1	79.8	92.5	107.4	95.2	109.9	94.0	48.2	55.9	54.2	56.1
Set 6 (Sulfide produced by <i>D. curvatus</i>)	5	69.9	70.3	78	81.8	96.3	93.6	95.0	93.8	54.7	56.2	51.3	61.4
	8	88.7	72.8	84.7	80.1	98.9	98.7	94.7	100.9	48.3	53.8	57.3	58.5
	15	83.6	68.3	74.7	73.7	99.4	95.7	93.8	100.9	52.6	56.9	52.6	53.4
	20	75.7	75.0	80.2	84.9	99.0	94.7	94.2	94.6	48.9	53.3	54.9	51.8

*Note: Four measurements for each phase for each time point.

Table S9. Extent of Fe(III) reduction for different experiments with 0.7 mM Si-HFO.

*Note: Four measurements for each phase for each time point.

Time (days)	Set 4 (<i>D. vulgaris</i>) (%)				Set 7 (Sulfide produced by <i>D. vulgaris</i>) (%)				Set 6 (Sulfide produced by <i>D. curvatus</i>) (%)			
5	33.4	34.3	36.0	36.3	64.3	68.8	63.6	71.3	66.1	66.5	63.2	70.5
8	40.2	42.4	41.6	43.5	64.1	72.3	61.7	68.9	61.4	64.9	66.9	69.1
15	37.5	36.3	37.8	35.7	64.1	71.0	61.5	67.8	64.0	66.1	63.4	65.6
20	34.7	37.2	34.9	35.7	63.6	68.5	69.5	68.4	63.3	65.1	66.5	65.1

Table S10. Measured Fe isotope compositions for aqueous, sorbed and solid phases in different experiments.

	Extent of reduction (%)	Aqueous		Sorbed		Solid	
		$\delta^{56}\text{Fe}$ (‰)	2SD	$\delta^{56}\text{Fe}$ (‰)	2SD	$\delta^{56}\text{Fe}$ (‰)	2SD
Set 4 (<i>D. vulgaris</i>)	33.4	N/A	N/A	N/A	N/A	0.27	0.004
						0.25	0.005
	37.2	-1.60	0.006	0.35	0.004	0.27	0.004
				0.47	0.004		
	37.8	-1.63	0.003	N/A	N/A	N/A	N/A
	40.2	-1.05	0.004	0.20	0.003	0.30	0.003
						0.25	0.004
	41.6	0.03	0.003	N/A	N/A	0.12	0.005
						0.21	0.004
						0.26	0.004
42.4	-0.91	0.004	0.23	0.004	0.31	0.004	
			0.18	0.004			
			0.28	0.003			
43.5	0.04	0.003	0.09	0.003	0.50	0.004	
	0.05	0.004			0.50	0.004	
Set 7 (sulfide produced by <i>D. vulgaris</i>)	61.5	-2.18	0.005	-0.18	0.004	0.47	0.003
		-2.11	0.004				
	64.3	-1.84	0.004	N/A	N/A	0.39	0.004
	67.8	-1.55	0.005	N/A	N/A	0.25	0.004
						0.33	0.004
	68.5	-1.68	0.004	-0.27	0.004	0.45	0.004
		-1.53	0.004	-0.22	0.004	0.28	0.004
	71.0	-0.71	0.005	-1.18	0.004	0.49	0.004
						0.33	0.004
	72.3	-0.50	0.005	-0.81	0.004	0.95	0.004

*Note: a) N/A means not available.

- b) Iron isotope compositions were directly measured for aqueous, sorbed and solid phases.
- c) Some duplicate analyses were determined for the same extent of Fe(III) reduction.
- d) 2SD is external precision based on three analyses of the same sample solution.

Table S11. Fe isotope compositions and Fe isotope fractionations for aqueous, sorbed and solid phases in different experiments.

	Extent of reduction (%)	Aqueous		Sorbed		Solid		$\delta^{56}\text{Fe}_{\text{aq}^-}$	$\delta^{56}\text{Fe}_{\text{aq}^-}$	$\delta^{56}\text{Fe}_{\text{sorb}^-}$	$\delta^{56}\text{Fe}_{\text{(II)}_{\text{aq}^-}}$
		$\delta^{56}\text{Fe}$ (‰)	2SD	$\delta^{56}\text{Fe}$ (‰)	2SD	$\delta^{56}\text{Fe}$ (‰)	2SD	$\delta^{56}\text{Fe}_{\text{sorb}}$ (‰)	$\delta^{56}\text{Fe}_{\text{solid}}$ (‰)	$\delta^{56}\text{Fe}_{\text{solid}}$ (‰)	$\delta^{56}\text{Fe}_{\text{(III)}_{\text{solid}}}$ (‰)
Set 4 (<i>D. vulgaris</i>)	33.4	N/A	N/A	N/A	N/A	0.26	0.03	N/A	N/A	N/A	N/A
	37.2	-1.60	N/A	0.41	0.17	0.27	N/A	-2.01	-1.87	0.14	-0.04
	37.8	-1.63	N/A	N/A	N/A	N/A	N/A	N/A	N/A	N/A	N/A
	40.2	-1.05	N/A	0.20	N/A	0.28	0.07	-1.25	-1.33	-0.08	-0.32
	41.6	0.03	N/A	N/A	N/A	0.20	0.14	N/A	-0.17	N/A	N/A
	42.4	-0.91	N/A	0.23	0.10	0.31	N/A	-1.14	-1.22	-0.08	-0.33
	43.5	0.05	0.01	0.09	N/A	0.50	0.00	-0.04	-0.45	-0.41	-0.86
Set 7 (sulfide produced by <i>D. vulgaris</i>)	61.5	-2.14	0.10	-0.18	N/A	0.47	N/A	-1.96	-2.61	-0.65	-1.22
	64.3	-1.84	N/A	N/A	N/A	0.39	N/A	N/A	-2.23	N/A	N/A
	67.8	-1.55	N/A	N/A	N/A	0.29	0.11	N/A	-1.84	N/A	N/A
	68.5	-1.60	0.21	-0.25	0.07	0.36	0.24	-1.35	-1.96	-0.61	-2.60
	71.0	-0.71	N/A	-1.18	N/A	0.41	0.23	0.47	-1.12	-1.59	-3.72
	72.3	-0.50	N/A	-0.81	N/A	0.95	N/A	0.31	-1.45	-1.76	-4.14

*Note: a) N/A means not available.

b) Iron isotope fractionations were calculated according to the method in section 4.3.

c) 2SD is two standard deviation based on two analyses. If only one set was performed for an extent of reduction, 2SD is N/A.

Cell transfer protocol for *Desulfobacter curvatus*

Work station

Turn on N₂ gas, use fresh pink syringe and needle with cotton inside. Flush sterile syringe and needle 3 times and get rid of one full syringe of N₂ each time and then flush with N₂ back and forth 6 to 7 times. If using 10 ml syringe, flush syringe 5 times fully. Before inserting needle into each bottle or tube, put alcohol to the cap and then flame it.

Freezing culture

Prepare a deoxygenated preserving medium by adding 3 ml glycerol into 7 ml fresh growth medium. Choose a rapidly and robustly growing *D. curvatus* culture (i.e., the optical density is higher than 0.5) to be frozen. Concentrate the biomass by centrifugation in the glove box at 8000 rpm for 10 min, and then re-suspend cells in the deoxygenated preserving medium. Mix the cells and medium well, and then separate the culture into 10 fisherbrand microcentrifuge tubes (2 ml) with screw cap o-ring and attachment loop (sterile ones) (1 ml for each tube) inside the clean bench (spray alcohol to surface of the bench and wipe it out and then turn on UV light for 10 min before using the bench). Close it quickly and put them inside the -80 °C freezer. Store them in a box with label on after freezing them.

Defreeze *D. curvatus* from stock culture in acetate. Transfer 1 ml above culture to 9 ml ATCC 1648 medium, add 0.15 ml 2 M sodium acetate, 0.1 ml 2 M Na₂SO₄, and 0.1 ml reducing agent 2 M Na₂S (to reduce any O₂ present) (1st culture). Incubate the 1st culture for 3 to 4 days at 30 °C. If cells are healthy, they will grow in 1 day, and the culture will turn more turbid from the morning to the afternoon in an acetate culture.

2nd transfer: add 1 ml 1st culture to 9 ml ATCC 1648 medium, 0.15 ml 2 M sodium acetate, 0.1 ml 2 M Na₂SO₄, and 0.1 ml 2 M Na₂S (2nd culture). Incubate for 3 to 4 days at 30 °C (3% to 5% transfer instead of 10% transfer will take longer but makes a more robust culture).

3rd transfer: add 1 ml 2nd culture to 2 tubes containing 9 ml ATCC 1648 medium, 0.15 ml 2 M sodium acetate, 0.1 ml 2 M Na₂SO₄, and 0.1 ml 2 M Na₂S (3rd culture). Incubate for 3 to 4 days at 30 °C.

4th transfer: add 10 ml 3rd culture to 2 bottles of 90 ml ATCC 1648 medium (number of bottles depends on how many cells are needed), 1.5 ml 2 M sodium acetate, 1 ml 2 M Na₂SO₄, and 1 ml 2 M Na₂S (can also do 1% transfer instead of 10% to make the culture more robust, which is important if more time is needed to set up the experiment).

Note: always add reducing agent first, then wait for ~2 hours before adding culture.

Cell transfer protocol for *Desulfovibrio vulgaris*

Work station

Same as cell transfer protocol for *D. curvatus*.

Freezing culture

Frozen culture was prepared by following the same steps as *D. curvatus*.

Defreeze *D. vulgaris* from stock culture in lactate. Transfer 1 ml above culture to 9 ml simple lactate medium, add 0.1 ml 2 M sodium lactate, 0.08 ml 2 M Na₂SO₄, and 1 drop reducing agent 0.17 M Na₂S (to reduce any O₂ present) (1st culture). Incubate the 1st culture for 3 to 4 days at 30 °C. If cells are healthy, they will grow in 1 day, and the culture will turn more turbid from the morning to the afternoon in a lactate culture.

2nd transfer: add 1 ml 1st culture to 9 ml simple lactate medium, 0.1 ml 2 M sodium lactate, 0.08 ml 2 M Na₂SO₄, and 1 drop 0.17 M Na₂S (2nd culture). Incubate for 3 to 4 days at 30 °C (3% to 5% transfer instead of 10% transfer will take longer but makes a more robust culture).

3rd transfer: add 1 ml 2nd culture to 2 tubes containing 9 ml simple lactate medium, 0.1 ml 2 M sodium lactate, 0.08 ml 2 M Na₂SO₄, and 1 drop 0.17 M Na₂S (3rd culture). Incubate for 3 to 4 days at 30 °C.

4th transfer: add 10 ml 3rd culture to 2 bottles of 90 ml simple lactate medium (number of bottles depends on how many cells are needed), 1 ml 2 M sodium lactate, 0.8 ml 2 M Na₂SO₄, and 0.1 ml 0.17 M Na₂S (can also do 1% transfer instead of 10% to make the culture more robust, which is important if more time is needed to set up the experiment).

Note: always add reducing agent first, then wait for ~2 hours before adding culture.

Acridine Orange (AO) Staining Instructions

Method developed by Christina Smeaton, Christine Ridenour and Maria Mesquita, and modified by Yan Zhang

1. Add a few drops of water to each filtration well (this helps the filters stick better to the mesh).
2. Add the nucleopore filters to the base of the filtration unit (wire mesh) in the following order:
 - a) 5.0 mm
 - b) 0.2 mm black (it looks grey, use the shiny side up)
3. Add the weights on top of the filters.
4. Close the valve on each filtration well, add a small amount of water (1 ml) to each filtration well, turn on the vacuum and let water pass through the well.
5. Close the valve on each filtration well.
6. Take out 0.1 ml culture from each tube, and add 100 ul culture to 900 ul PBS (phosphate buffered saline; prepared by adding 0.4 g NaCl, 0.01 g KCl, 0.072 g NaH₂PO₄, and 0.012 g KH₂PO₄ into 40 ml H₂O and adjust the pH from 4.6 to 7.4 by adding 0.5 ml 1 M NaOH. Then add water to get a final volume of 50 ml. Autoclave the solution for 30 min at 121 °C under liquid system, and store at room temperature) and vortex bacteria at 3000 rpm for 15 sec to ensure uniform cell distribution, and then add 0.1 ml 25% glutaraldehyde into the cell suspension.
7. Carefully pipette whole 1.1 ml cell suspension to each well by adding it to the side of the chimney of each unit.
8. Carefully add 100 ul of 1 g/l of AO to the side of the chimney of each well.
9. Gently shake the unit.
10. Wait 3 minutes.
11. Add 900 ml of PBS.
12. Turn on the vacuum pump.
13. Open the valves on each filtration unit.

14. Let the solution run through until you don't see any more liquid (wait 30 sec after the last drop to ensure it is completely filtered).
15. Turn off vacuum pump.
16. Close the valves on each filtration unit.
17. Rinse the sides of the chimney well (particularly where you added your cells and AO) with 2 ml of water.
18. Open the valves on each filtration unit.
19. Turn on the vacuum pump.
20. Let the solution run through until you don't see any more liquid (wait 30 sec after the last drop to ensure it is completely filtered).
21. Repeat step 17-20.
22. Remove the filtration weights.
23. Add 10 μ l of DABCO reagent to the bottom of a glass slide. DABCO helps to maintain the fluorescence of the strain.
24. Carefully place your filter paper on top of the drop (avoid getting air bubbles in the filter paper).
25. Add another 10 μ l of DABCO to the top of the filter paper.
26. Carefully place the slide cover on top of the filter paper.
27. Note: 2 filter papers can be put on one glass slide. If you want to keep your sample, you can paint the edge of each slide cover with clear nail polish to prevent your sample from drying out.